Association between $CD4^+$ T cell hyperfunction and advanced liver injury in chronic liver disease

Natasha Campeau

Thesis submitted to the University of Ottawa in partial fulfillment of the requirements for the degree of Master of Science in Microbiology and Immunology

Dept. of Biochemistry, Microbiology, and Immunology
Faculty of Medicine
University of Ottawa

© Natasha Campeau, Ottawa, Canada, 2024

ABSTRACT

Chronic liver disease accounts for more than 2 million annual deaths worldwide and falls within the top 20 leading causes of death. Particularly, metabolic dysfunction-associated steatohepatitis (MASH) is now the leading cause of end-stage liver disease, surpassing viral hepatic infections. Over time, liver fibrosis impacts organ structures and function, and is increasingly associated with local and circulating immune cell dysfunction and systemic inflammation, collectively contributing to poor clinical outcomes. This thesis aimed to investigate $CD4^+$ T cell function in the context of chronic liver disease in humans and in murine models that mimic HCV and MASLD pathologies. We hypothesized that in chronic liver disease, $CD4^+$ T cell hyperfunction and increased intrahepatic infiltration are associated with advanced liver injury. In MASH patients, we found $CD4^+$ T cell hyperfunction in those with advanced liver fibrosis, marked by increased TGF-β and IFN-γ production. Data collected from the diet-induced liver model suggest sex differences with transient $CD4^+$ T cell hyperfunction in males, while hyperfunction in females sustained until 2 weeks post-HFMCDD cessation, characterized by elevated GrzB and IFN-γ expression. In addition to these findings, positive correlations were also observed between $CD4^+$ and $CD8^+$ T cell infiltration and liver injury severity. In conclusion, these findings suggest an association between $CD4^+$ T cell hyperfunction and advanced liver injury in chronic liver disease.

ACKNOWLEDGEMENTS

Firstly, I would like to thank my supervisor Dr. Angela Crawley for being a patient and supportive teacher and mentor, helping me improve not only my scientific research skills, but also my interpersonal skills. She made sure that I obtained all the necessary skills and training required to succeed in this field, as well as pushed me to engage in critical thinking. I am grateful for all the one-on-one support, continuous encouragement and feedback throughout my graduate studies.

My deepest gratitude goes to my colleagues in the Crawley lab: namely, Katrina Jorritsma for her leadership in completing animal work associated with her MSc project on $CD8^+$ T cells, including blood collection, sample processing, staining and flow cytometry; Jeff Li, who provided valuable insight and advice regarding scientific experiments, as well as lending a hand with the animal models; and David Lawton, who contributed significantly in the optimization, development and completion of the triple IF experiments, and helped with many of the mouse experiments. Most importantly, I would like to thank all the aforementioned colleagues for their never-ending understanding, support and encouragement during my graduate studies. Furthermore, I would also like to thank our research associates, Dr. Agatha Vranjkovic PhD and Dr. Torki Alothaimeen PhD, for their training, guidance and help with both human and mouse model research activities.

I would also like to thank the members of my thesis advisory committee, Drs. Michele Ardolino and Angela Cheung for their guidance and feedback regarding animal and human studies, respectively. The support they provided at the yearly committee meetings allowed me to, not only improve my research skills, but also expand my critical thinking abilities.

I would like to thank everyone at the University of Ottawa Louise Pelletier Histology Core, namely Sharlene Faulkes, who helped with the design, troubleshooting and execution of the triple immunofluorescence immunohistochemistry experiments. And lastly, I would like to extend gratitude to those who helped from the University of Ottawa Flow Cytometry and Virometry Core and the Animal Care and Veterinary Services Facility.

Table of Contents

LIST OF TABLES

LIST OF FIGURES

LIST OF ABBREVIATIONS

ALD – Alcohol-related liver disease

CCl_3^- - Trichloromethyl

CCl_4 – Carbon tetrachloride

CLD – Chronic liver disease

CTLA-4 – Cytotoxic T-lymphocyte antigen 4

DAAs – Direct-acting antivirals

ECM – Extracellular matrix

FFPE – Formalin-fixed paraffin-embedded

FMO – Fluorescence minus one

GLP-1 – Glucagon-like peptide-1

GrzB – Granzyme B

HBV – Hepatitis B virus

HCC – Hepatocellular carcinoma

HCV – Hepatitis C virus

HFHC – High-fat high-cholesterol

HFMCDD – High-fat, methionine-deficient, choline-deficient diet

HIV – Human immunodeficiency virus

HSC – Hepatic stellate cells

H&E – Hematoxylin and Eosin

IF – Immunofluorescence

IFN-γ – Interferon gamma

IL-2 – Interleukin 2

IL-6 – Interleukin 6

IL-10 – Interleukin 10

IL-17 – Interleukin 17

IL-21 – Interleukin 21

KC – Kupffer cells

kcal - Kilocalorie

kPa – Kilopascals

LAG-3 – Lymphocyte activation gene 3 protein

MASH – Metabolic dysfunction-associated steatohepatitis

MASL – Metabolic dysfunction-associated steatotic liver

MASLD – Metabolic dysfunction-associated steatotic liver disease

MCD – Methionine choline deficient

MT – Masson's trichrome

NK – Natural killer cells

PBMC – Peripheral blood mononuclear cells

PBS – Phosphate buffered saline

PD-1 – Programmed cell death protein 1

PD-L1 – Programmed death-ligand 1

PDGF – Platelet-derived growth factor

ROS – Reactive oxygen species

STAT3 – Signal transducer and activator of transcription 3

SVR – Sustained virological response

T2DM – Type 2 diabetes mellitus

TGF-β – Transforming growth factor beta

Th17 – Type 17 T helper cell

THRβ – Thyroid hormone receptor β selective agonist

TIM- 3 – T cell immunoglobulin and mucin-domain containing-3

TNF-α – Tumour necrosis factor alpha

Tregs – Regulatory T cells

CHAPTER 1: INTRODUCTION

1.1 Burden of chronic liver disease

Chronic liver disease (CLD), which progresses in four stages: hepatitis, fibrosis, cirrhosis and liver failure, account for approximately 2 million deaths per year or 4% of all deaths globally[1,2]. The majority of deaths are attributable to cirrhosis complications, such as portal hypertension, esophageal varices, hepatic encephalopathy, ascites and hepatocellular carcinoma (HCC)[3]. As the third leading cause of cancer-related deaths worldwide, HCC accounts for about 75-85% of primary liver cancer cases[4]. The main causes of CLD include chronic viral hepatitis, such as hepatitis B and C infections (HBV and HCV, respectively), alcohol-related liver disease (ALD) and metabolic dysfunction-associated steatotic liver disease (MASLD, formerly known as non-alcoholic fatty liver disease, NAFLD). According to the World Health Organization, approximately 130-150 million people have chronic HCV infection and of those, 500 000 succumb to HCV-related liver diseases[5].

The prevalence of MASLD has now surpassed viral hepatitis as the main cause for end-stage liver disease, affecting more than 32% of the world's population. This shift is largely due to highly effective direct-acting antiviral (DAA) therapies that can cure HCV and the globally increasing prevalence of obesity, cardiovascular diseases, metabolic disorders and type 2 diabetes mellitus (T2DM)[6,7]. MASLD is the most common liver disorder in Western countries, affecting 31% of adults, and of those diagnosed, 20-30% develop metabolic dysfunction-associated steatohepatitis (MASH, formerly known as non-alcoholic steatohepatitis (NASH)), the advanced inflammatory form of MASLD[8,9]. In chronic HCV and MASH, liver fibrosis progresses to cirrhosis over time, increasing the risk of HCC. Twenty percent of chronic HCV-infected individuals will develop cirrhosis within a few decades, of which, approximately 4% will progress to HCC annually[10,11].

Similarly, in MASH, over a 20-year period, an estimated 10% of individuals will progress to cirrhosis, and 2.6% of these individuals will develop HCC[12,13].

1.2 HCV infection

1.2.1 HCV infection & disease progression

HCV is a blood-transmitted virus that predominantly targets hepatocytes and hematopoietic cells, such B lymphocytes, in which its genome gets replicated[14]. The virus is transmitted through contact with infected blood, as seen through sharing needles and syringes, unsafe blood transfusions, unprotected sexual practices or mother-to-baby vertical transmission[5]. HCV infection can either be acute, when the period of inflammation and liver insult is less than six months and there is viral clearance, or chronic, when viremia persists beyond six months[15]. Approximately 25% of those infected will spontaneously clear the virus within 6 months, while the majority (75%), if left untreated, will develop chronic HCV infection, at which point, risks of cirrhosis and HCC increase significantly[15,16]. Viral clearance is associated with the development and persistence of strong virus-specific responses by $CD8^+$ cytotoxic T lymphocytes and $CD4^+$ helper T cells. However, in most infected individuals, viremia persists due to altered HCV-specific $CD8^+$ T cell responses and loss of HCV-specific $CD4^+$ T cells, while accompanied by variable degrees of hepatic inflammation and fibrosis[17,18]. In chronic HCV infection, there is persistent, uncontrolled inflammation, which subsequently activates hepatic stellate cells (HSCs) to secrete and deposit extracellular matrix (ECM) proteins, such as collagen, in the liver[19]. The liver undergoes many rounds of wound healing to repair the tissue damage caused by the excessive accumulation of collagen (fibrotic scar). Over time, liver fibrosis impacts organ structures and function, and is increasingly associated with immune dysfunction and systemic inflammation, collectively contributing to poor clinical outcomes[20].

HCV infection diagnosis is made using a serological test, searching for anti-HCV antibodies, followed by a nucleic acid test to confirm chronicity. This secondary test is vital as the 25% of HCV-infected individuals who spontaneously clear the infection without treatment will still test positive for anti-HCV antibodies. After these tests, liver biopsies or other non-invasive techniques, such as liver elastography (Fibroscan®), will be performed to assess the degree of liver damage (fibrosis and cirrhosis)[17]. The main goal of HCV treatment is to cure the disease or prevent long-term liver damage. The first-line standard-of-care treatment for HCV infection are DAAs, such as telaprevir and sofosbuvir, which can achieve sustained virological response (SVR) or HCV cure in over 90% of HCV-infected individuals[21]. In HCV-infected individuals with advanced liver fibrosis, DAAs can reduce portal hypertension, improve liver dysfunction and metabolic disorders, and promote fibrosis regression after SVR[22,23]. DAAs target HCV-encoded proteins, disrupting specific steps within the HCV life cycle, such as viral entry, protein translation, RNA replication, viral assembly and release. A multitude of DAAs have been developed and divided into four classes, depending on their mechanism of action and therapeutic target within this cycle[24–26]. Although DAA therapy has proven to be effective, it does not, however, protect from HCV re-infection, or eliminate the risk of HCC in cirrhosis[21,27].

1.2.2 Immune response to HCV

Chronic HCV infection is associated with the persistent production of pro-inflammatory cytokines and chemokines by hepatocytes, Kupffer cells (KCs) and natural killer (NK) cells recruited to the liver[28,29]. These cytokines play a role in recruiting other immune cells, such as T cells, to the liver which further contribute to inflammatory responses, activating HSCs to secrete and deposit ECM, resulting in the formation of fibrotic tissue[20]. An array of factors contribute to T cell dysfunction in chronic viral infection, such as T cell exhaustion, viral escape mutations and

helper $CD4^+$ T cell deletion, contributing to viral persistence[27]. Persistent viremia is firstly met with robust and effective HCV-specific $CD8^+$ T cell responses, coordinated with strong support from HCV-specific $CD4^+$ helper T cells early in the acute phase. This is followed by a decline in functionality of HCV-specific $CD8^+$ T cells in addition to the deletion of HCV-specific $CD4^+$ T cells, thus failing to eliminate the virus and progressing to chronic HCV infection[18,30]. Prolonged stimulation by antigens contributes to T cell exhaustion, characterized by a loss of effector functions of HCV-specific $CD8^+$ and $CD4^+$ T cells and over-expression of inhibitory receptors, such as T cell immunoglobulin and mucin-domain containing-3 (TIM-3), programmed cell death protein 1 (PD-1), lymphocyte activation gene 3 protein (LAG3) and cytotoxic T-lymphocyte antigen 4 (CTLA-4), which have been extensively characterized in both mice and humans[18,27]. Another feature thought to strongly mediate $CD8^+$ T cell exhaustion is the expansion of regulatory T cells (Tregs), a $CD4^+$ T cell subset, which suppresses $CD8^+$ T cell activity[31]. As central mediators of adaptive immunity, $CD4^+$ T cells facilitate both $CD8^+$ T cell responses and B cell-mediated antibody responses to viral pathogens, as well as targeting infected cells through cytotoxic mechanisms. Cytotoxic $CD4^+$ T cells, which secrete profibrotic cytokines such as perforin and granzyme B, have been found to participate in viral clearance and fibrogenesis in hepatic viral infections and HIV[32,33]. The deletion of HCV-specific $CD4^+$ T cell responses may be a significant driver of $CD4^+$ T cell failure and $CD8^+$ T cell dysfunction in chronic HCV infection[34,35]. Several studies have demonstrated reduced or absent HCV-specific $CD4^+$ T cell responses, during chronic HCV infection, with a failure of interleukin 2 (IL-2) secretion that may lead to disruption of interferon gamma (IFN-γ) and cellular proliferation[31,36].

1.2.3 Sex differences in HCV infection

Once exposed to HCV, men demonstrate a higher prevalence of HCV viremia, characterized by elevated HCV RNA levels, reduced viral clearance and faster rates of disease progression[37,38]. In postmenopausal women, when levels of estrogen drop significantly, there is a reduction in viral clearance, leading to increased rates of fibrosis. Estrogens have a protective role in the liver, shielding hepatocytes from oxidative stress, inflammatory injury, and cell death, contributors to fibrosis, as well as suppressing hepatocarcinogenesis[39,40]. In addition, estradiol somewhat protects the liver against sustained injury, by preventing the accumulation of monocytes and macrophages in hepatic tissue, thus inhibiting the production of reactive oxygen species (ROS) and proinflammatory cytokines, and subsequently, the proliferation and activation of HSCs[41]. In a study focusing on the effect of estrogens on women with chronic HCV infection, it was shown that history of pregnancy and exposure to hormone replacement therapy are associated with decreased fibrosis progression. For example, women taking oral contraceptives had lower fibrosis scores[42]. Furthermore, a study by Florian et al. demonstrated that men with chronic HCV infection have a greater decrease in liver enzymes (e.g. AST and ALT) after antiviral treatment compared to women, indicated improved liver function[43].

1.3 MASLD

1.3.1 MASLD pathogenesis & diagnosis

As the most common cause of CLD, MASLD rates mirror the increasing incidence of obesity and T2DM, with a global and North American prevalence of approximately 30% in adults[44,45]. MASLD is characterized by excessive hepatic lipid accumulation in addition to at least one cardiometabolic risk factor, and where alternative causes, such as viral hepatitis and excessive alcohol intake have been excluded[46]. MASLD constitutes a range of chronic liver diseases, from

simple steatosis (termed metabolic dysfunction-associated steatotic liver, MASL) to the inflammatory version of the disease, MASH, to fibrosis, cirrhosis and eventually, HCC[47,48]. While fat accumulation in the liver can be controlled or reversed by adopting healthier lifestyle changes, MASL could progress to MASH when left uncontrolled, characterized by hepatocellular ballooning, tissue degeneration, inflammation and fibrosis[49]. The pathophysiology of MASLD involves increased fatty acid synthesis and impaired inhibition of adipose tissue breakdown, ensuing the increased delivery and subsequent accumulation of fatty acids in the liver. The resulting lipotoxicity causes metabolic dysfunction and insulin resistance, prompting the secretion of adipokines and proinflammatory cytokines, immune cell infiltration and fibrogenesis[50]. Ultimately, these processes induce oxidative stress and DNA damage to hepatocytes, which, in combination with inflammation, further promote the development of fibrosis and cirrhosis[51,52].

MASLD diagnosis includes the use of a variety of techniques. Firstly, serology occurs to perform liver function tests (e.g. AST, ALT, ALP) and to rule viral hepatic infections, such as HBV or HCV. This is followed by liver imaging tests (e.g. ultrasonography, CT and MRI), to identify the degree of hepatic injury, focusing on hepatic steatosis[53]. Ultrasound elastography is another widely used non-invasive test for the assessment of liver stiffness, however, it cannot differentiate between MASLD and MASH, or exclude other causes (e.g. alcohol intake) for the liver damage[54,55]. The gold standard for MASLD/MASH diagnosis is a liver biopsy, which can rule out alternative diseases (e.g. autoimmune hepatitis, primary biliary cholangitis, primary sclerosing cholangitis, etc.) and confirm fatty liver disease as the cause of liver damage, as well as differentiate all stages of steatosis, inflammation and fibrosis[56].

After diagnosis, management of MASLD includes lifestyle modifications, primarily diet and exercise, to reduce body weight, and pharmaceutical therapies such as GLP-1 modulators to

target molecular pathways involved in MASH[53,57,58]. Developing pharmaceutical therapies for MASH has been challenging, seeing that in order to effectively treat MASH, the drug needs to address fat accumulation, inflammation and fibrosis, and none have been able to meet all of these criteria thus far. In early 2024, the FDA in the United States approved a new oral therapeutic drug, called resmetirom, a liver-targeted thyroid hormone receptor β selective agonist (THRβ), which controls fat synthesis, regulates fatty acid oxidation, cholesterol metabolism, and reduces both inflammation and fibrosis[59]. Preliminary studies for resmetirom demonstrated MASH resolution with no worsening of fibrosis in 25-30% of treated patients, and fibrosis improvement by at least one stage with no worsening of MASLD in 24%[60,61]. Although this medication demonstrates great potential towards resolving MASH-associated liver injury, it, unfortunately, remains inaccessible to Canadians[62]. The preferred treatment for MASH, as of yet, has been glucagon-like peptide-1 (GLP-1) receptor agonists, which are approved for the treatment T2DM and/or obesity. These drugs have also been used to treat MASLD/MASH, as they target metabolic defects and lipotoxicity prevalent in all three diseases[59,63]. Extensive research into MASH treatment continues to take place, investigating a multitude of pathways, such as other thyroid hormone receptors, hepatic steatosis synthesis, inflammatory pathways and many more[64].

1.3.2 Immune response to MASLD

Non-resolving inflammation occurs when the inflammatory stimuli persist or the regulatory mechanisms are disrupted, amplifying pathological consequences such as fibrosis and HCC[65]. When left untreated, chronic inflammation contributes to the progression of MASLD to MASH[66]. In MASLD, studies have shown that $CD4^+$ T cells promote liver inflammation and fibrosis by producing proinflammatory cytokines, such as interleukin 17 (IL-17) and IFN-γ, and by activating HSCs[67,68]. In the liver, IL-17 primarily targets HSCs by activating the STAT3 signaling pathway,

and promoting the production and deposition of type I collagen[69]. Interestingly, a positive correlation was found between subsets of peripheral $CD4^+$ T cell subsets (Th1 and Th17) and the MASLD Activity Score, which measures steatosis, hepatocyte ballooning and lobular inflammation[70]. A humanized mouse model for diet-induced MASLD showed that subsets of $CD4^+$ T cells, specifically IL-17-secreting Th17 and IFN-γ-secreting Th1 cells, play a key role in the progression of steatosis to fibrosis and correlate positively with disease progress in MASH-HCC. It is also important to note that Tregs inhibit the function of Th1 cells, thus impairing immunosurveillance in the MASH liver[71,72]. Therefore, the balance between Th17 and Tregs within the liver is vital as Tregs may relieve liver inflammation but also impair cancer immunosurveillance provided by T cells in the later stages of MASLD[73,74]. Further inducing excessive collagen secretion and tissue dysfunction, cytotoxic $CD4^+$ T_{EM} cells, characterized by increased perforin and GrzB expression, have been found in the livers of MASLD patients[75]. In addition, bulk $CD8^+$ T cells that display an activated-exhausted phenotype ($CXCR6^+PD\text{-}1^+$), have been shown to promote MASLD progression by inducing inflammation, hepatocyte death and fibrosis, through the secretion of TNF-α, IFN-γ, perforin and granzymes[76,77].

1.3.3 Sex differences in MASLD/MASH

Many studies over the last decade have highlighted the heterogeneity that exists between males and females in the prevalence and mechanisms of MASLD. In the general adult population, MASLD prevalence is higher in men than in women, with a prevalence of 18.5% and 10.3%, respectively[78,79]. Furthermore, males are more susceptible to developing MASH, fibrosis and cirrhosis, and are diagnosed with HCC two to four times more often than females.[80] These sex differences are age-related, as adult men (<50 years old) typically develop MASLD, while women are more likely to develop MASLD after menopause (>50 years old), with most exhibiting clinical

symptoms around 60–70 years of age. Therefore, premenopausal women have reduced risks of MASLD compared to men, whilst postmenopausal women have comparable prevalence of MASLD as age-matched men[81,82]. Research has shown that sex hormones, specifically estrogens and progesterone, are responsible for these sex differences, as they influence many processes involved in the pathophysiology of MASLD. For example, estrogens exert a protective role on the liver by regulating lipid metabolism, suppressing inflammation, promoting tissue repair and regeneration, and regulating insulin release and glycogen synthesis[83–85]. In a menopause murine study, estrogen deficiency promoted insulin resistance and lipid synthesis, thus increasing hepatic lipid accumulation[86]. Prolonged estrogen deficiency in these mice and in postmenopausal women diagnosed with MASLD, was associated with amplified proinflammatory responses and oxidative stress, and the development of MASH[87]. Similarly, progesterone can modulate insulin sensitivity and adipose tissue function[88].

1.4 T cell dysfunction in chronic liver disease

During chronic viral infections, such as HCV and HBV, pathogen persistence is thought to continuously stimulate antigen-specific T cells. These T cells are driven into clonal deletion or exhaustion, thus inducing dysfunction and preventing adequate pathogen clearance[89,90]. Mainly, the reduced proliferative capacity and low IL-2, TNF-α and IFN-γ production by $CD4^+$ T cells, as well as impaired cytotoxicity of $CD8^+$ T cells are signs of effector function loss in T cells[91,92]. In chronic infection, it was found that IL-21 secretion by $CD4^+$ T cells maintained $CD8^+$ T cell function and helped facilitate viral control[93,94]. In patients with chronic HIV and HCV infections, where decreased frequency of IL-21-producing $CXCR5^+CD4^+$ T cells was observed, exhausted $CD8^+$ T cells entered a dysfunctional state, noted by an impairment in IL-2, IFN-y and TNF-α production[95,96]. It has, therefore, been demonstrated that high viral load and low availability of

$CD4^+$ T cells, during chronic HCV infection, correlate with severe T cell exhaustion[97]. In many viral infections and cancer, including HCV and HIV, antigen-specific exhausted $CD8^+$ T cells were observed to have distinct epigenetic signatures, termed "epigenetic scars", which persist long after viral clearance with DAA therapy[98]. In previous studies, the Crawley lab observed hyperfunction of bulk circulating $CD8^+$ T cells in individuals with chronic HCV infection, characterized by increased expression of IFN-γ and perforin, which persisted even after viral clearance with DAAs[99]. Similar results were observed in a hepatotoxin-induced liver fibrosis murine model, where the Crawley research team observed T cell hyperfunction, characterized by increased proportions of $GrzB^+$ and IFN-γ^+CD8^+ T cells[100]. These findings suggest a broader epigenetic scar, manifesting as a hyperfunctional signature in bystander $CD8^+$ T cells. Through RNA-sequencing, we were also able to identify altered expression of genes associated with $CD8^+$ T cell function, survival, cellular metabolism and cytoskeletal dynamics in HCV-infected individuals, suggesting the presence of an epigenetic scar[101]. In other chronic diseases, such as MASLD and MASH, selective loss of $CD4^+$ T cells has been observed, therefore, causing insufficient immune surveillance and impaired tumour growth[102]. In the Crawley lab, using a high-fat, methionine-deficient and choline-deficient murine model, mimicking MASLD pathophysiology, $CD8^+$ T cell hyperfunction was observed, characterized by increased proportions of $GrzB^+$ and IFN-γ^+CD8^+ T cells[103].

1.5 Intrahepatic T cell infiltration in chronic liver diseases

1.5.1 T cell infiltration in HCV infection

Following chronic liver injury, as seen in chronic HCV infection, infiltration of various types of immune cells, such as monocytes/macrophages, NK cells and T cells, is a central pathogenic feature[104]. The induction of inflammation following liver injury leads to the recruitment

and activation of leukocyte populations and promotion of fibrogenesis. These fibrotic responses are regulated by inflammatory cytokines (e.g. TNFα and IL-6), which in turn, activate HSCs, large producers of collagen[105]. A recent study demonstrated that extensive lymphocyte infiltration containing an abundance of activated $CD4^+$ Tregs was present in livers of chronic HCV-infected individuals, while absent from healthy livers[106]. A study by Ward et al. found that the intrahepatic infiltration of $CD4^+$ Tregs in chronic HCV infection reduces T cell responses, improving liver inflammation whilst promoting fibrotic processes[107]. Interestingly, it was observed that exhausted peripheral HCV-specific $CD8^+$ T cells are readily found in the liver, and subsequently, the site of viral replication[108]. These liver-infiltrating $CD8^+$ T cells express pro-inflammatory IL-10, and have been found to increase hepatic macrophage infiltration, and induce HSC activation. Furthermore, liver infiltrating $CD8^+$ T cells contribute to liver pathology by targeting virus-infected hepatocytes and inducing non-specific inflammatory responses[77,109].

1.5.2 T cell infiltration in MASLD

Diffuse lobular infiltration of immune cells is a key histological feature of MASLD/MASH, greatly contributing to inflammation regulation, maintenance of liver homeostasis, liver tissue remodeling, hepatocyte damage and the progression to HCC[110,111]. As MASLD progresses to MASH, there is a significant increase in infiltration of $CD4^+$ and $CD8^+$ T cells, as well as NK cells and macrophages[112]. In a recent high-fat high-cholesterol (HFHC) murine study, mimicking the histopathological features of MASLD, liver sections from the HFHC diet-fed mice showed significant increases in infiltrated $CD4^+$ and $CD8^+$ T cells, as well as macrophages ($CD68^+$), which generally localized to fibrotic regions. Similar results were observed in liver tissue from individuals with MASLD. The mouse and human results obtained from these studies suggest a role for $CD4^+$ T cells in diet-induced liver inflammation and steatosis-to-fibrosis

progression[72]. Interestingly, this mouse model indicated that intrahepatic infiltration of $CD8^+$ T cells and macrophages is driven by $CD4^+$ T cells, while the depletion of $CD4^+$ T cells reduced immune infiltration, inflammation and fibrosis. These findings are consistent with the previously mentioned role that $CD4^+$ T cells play in MASLD progression[113]. Furthermore, in both mouse models and MASH patients, the recruitment of activated cytotoxic $CD8^+$ T cells into the liver has been observed, promoting insulin resistance, immune-mediated liver damage, and fibrosis[114,115]. In a separate murine model, where C57BL/6 mice were fed a methionine and choline-deficient (MCD) diet for 8 weeks, mimicking the pathophysiology of MASH, they observed an increased frequency of $CD4^+$ T cells in liver tissue compared to controls[116]. More specifically, Th17 cells, a $CD4^+$ T cell subset, which secretes pro-inflammatory IL-17, have been found to accumulate in the liver of patients with MASH[117].

1.6 Animal models of chronic liver disease

1.6.1 Hepatotoxin-induced liver fibrosis

Since HCV cannot infect wild-type rodents, the hepatotoxin model using carbon tetrachloride (CCl_4) was developed to replicate HCV-induced liver fibrosis, in the absence of viral infection. CCl_4 is administered at regular intervals causing progressive liver damage and fibrosis, but not hepatic steatosis[118]. Hepatocytes metabolize CCl_4, forming free trichloromethyl (CCl_3^-) radicals, which damage hepatocytes by directly impairing the permeability of plasma, lysosomal and mitochondrial membrane, causing centrilobular necrosis[119,120]. This activates HSCs, which produce excessive collagen deposits in the ECM, thus leading to hepatic fibrosis[121]. Studies have shown that 8-20 weeks of intraperitoneal CCl_4 injections twice weekly are sufficient to induce fibrosis with central-portal bridging, eventually leading to cirrhosis. Repeated liver insult from

frequent doses of CCl_4, and successive rounds of wound healing result in the accumulation of fibrotic tissue[122].

1.6.2 HFMCDD-induced liver injury

There are numerous dietary mouse models that induce hepatocellular steatosis, but the high-fat methionine and choline deficient diet (HFMCDD) model closely mimics the histopathological features of human MASLD and MASH[123]. In order to accurately replicate the features of steatohepatitis, there needs to be evidence of ballooning hepatocyte degeneration in addition to fat accumulation and inflammation[124]. The combination of a high-fat diet and methionine and choline deficiencies overcomes the limitations of other high-fat diet models by inducing steatohepatitis, liver fibrosis and eventually HCC, without causing any loss of body weight in mice[125]. In C57BL/6 mice, moderate inflammation and ballooning with advanced steatohepatitis (S3) are expected after 3 weeks of feeding, followed by moderate (F1-2) and advanced liver fibrosis (F3) by 6-9 and 12 weeks of feeding, respectively[126].

1.7 Rationale & Hypothesis

Research has demonstrated that the deletion of HCV-specific $CD4^+$ T cell responses may be a contributing factor to $CD8^+$ T cell dysfunction in chronic HCV-infection[19,35]. Prior studies in the Crawley lab have clearly demonstrated that $CD8^+$ T cells are hyperfunctional in chronic HCV infection with advanced liver fibrosis, which persists long after viral clearance with DAA therapy[99,100]. In a CCl_4-induced liver injury murine model, mimicking chronic HCV infection pathology, we found that C57BL/6 mice expressed hyperfunctional $CD8^+$ T cells, characterized by elevated GrzB and IFN-γ expression, as well as $CD4^+$ T cell hyperfunction, characterized by increased proportions of $GrzB^+CD4^+$ T cells[100]. In a second murine model, the HFMCDD-induced

liver injury that mimics MASLD pathophysiology was associated with T cell hyperfunction, characterized by increased proportions of $GrzB^+$ and IFN-γ^+CD8^+ T cells, was observed[103]. Although, decades of literature have outlined the important role that $CD4^+$ T cells play in the MASLD progression of steatosis-to-fibrosis, the presence of $CD4^+$ T cell dysfunction, and the mechanisms that underly it, have yet to be characterized[72,102,116]. Studying $CD4^+$ T cell activity and function across various etiologies of liver injury will provide valuable insight into identifying unique and shared features associating liver disease severity with generalized immune cell function, as well as identifying actionable targets for the treatment of disease.

Hypothesis: Generalized $CD4^+$ T cell hyperfunction is associated with advanced liver injury in chronic liver disease

1.8 Objectives

2. Evaluate $CD4^+$ T cell function in human MASH
3. Assess $CD4^+$ T cell function in established murine models of liver fibrosis
4. Analyze T cell infiltration in established murine models of liver fibrosis

CHAPTER 2: MATERIALS & METHODS

2.1 MASH participants

Individuals included in this study were healthy or patients diagnosed with MASH with varying degrees of liver fibrosis. Number, gender, mean age are summarized in Table 1. Collection of blood and liver biopsy tissue from human subjects were completed as part of clinical studies lead by Drs. Curtis Cooper (Scientist at the OHRI in the Inflammation and Chronic Disease program, and Director of the Ottawa Hospital and Regional Hepatitis Program) and Angela Cheung (Associate Scientist at OHRI in the Inflammation and Chronic Disease program, Hepatologist at TOH). Fibrosis severity was determined by liver elastography, and individuals were grouped by fibrosis stage (F0-1 or F4) after sample collection. For those who received liver biopsies, the METAVIR scoring system, an algorithm for the evaluation of histological activity and fibrosis range description, was used on hepatic tissue to stage the disease.

Table 1: Baseline characteristics of study participants

	Healthy control	MASH with minimal fibrosis	MASH with advanced fibrosis
n	7	7	5
Gender[a]	3M, 4F	3M, 4F	2M, 3F
Mean Age	36.7 ± 5.5	46.9 ± 18.1	63.0 ± 5.8
Mean Age per Sex	M: 38.8 ± 6.4 F: 34.6 ± 4.6	M: 47.6 ± 16.9 F: 46.4 ± 20.2	M: 67.0 ± 1.4 F: 61.7 ± 6.2
Fibrosis Stage[b]		F0: 5 F1: 2	F4: 5
Mean kPa		7.0 ± 2.0	23.8 ± 11.1

[a] M(male), F(female)

[b] measured by Fibroscan

2.2 Animals

These projects follow the animal use protocol OHRIe-3003 with the University of Ottawa Animal Care and Veterinary Services (ACVS), certified by the Canadian Council on Animal Care. In all mouse experiments, C57BL/6 mice were purchased from Jackson Laboratory or bred in the ACVS facility at the University of Ottawa. Animals were aged between 7-10 weeks at the start of experiments. Animal studies are summarized in Table 2.

Table 2: Animal studies conducted

Study		# of mice	Sex	Treatment	Duration of treatment
CCl_4	E09	22	15M, 7F	M: 6 ctl, 9 CCl_4 F: 3 ctl, 4 CCl_4	21 weeks
	E10	23	12M, 11F	M: 6 ctl, 6 diet F: 5 ctl, 6 diet	15 weeks
HFMCDD	E01	21	M	9 ctl, 12 diet	21 + 4 weeks regression
	E02	19	F	7 ctl, 12 diet	21 + 4 weeks regression
	E03	24	12M, 12F	M: 6 ctl, 6 diet F: 7 ctl, 5 diet	17 weeks

CCl_4: carbon tetrachloride

HFMCDD: high-fat methionine-deficient, choline-deficient diet

[a] M(male), F(female)

2.3 CCl_4 murine model

In this murine model of hepatotoxin-induced liver fibrosis, C57BL/6 mice were injected (i.p) twice weekly, for 15-21 weeks, with 0.1mL of CCl_4 (≥99.5%, anhydrous, Sigma-Aldrich, MO, USA) at a concentration of 1.0mL/kg of body weight diluted in filtered olive oil (Bertolli)[100]. Control mice were injected with olive oil alone. Throughout the studies, body weight and overall physical condition were carefully monitored for signs of distress (≥20% loss in body weight, reduced mobility, piloerection and/or hunching) to justify humane endpoint if necessary.

2.4 HFMCDD murine model

In this murine model of diet-induced liver fibrosis, C57BL/6 mice were placed on a high-fat methionine-, choline-deficient diet (HFMCDD) composed of 60% kcals fat, 0.1% methionine and no added choline (A06071302, Cedarlane, ON, CAN) *ad libitum* for 17-21 weeks[127]. To maintain humane living conditions, animal cages and diet pellets were changed 2-3 times weekly due to the high lard pellet content, causing rapid breakdown and soiling. Control mice were placed on the standard chow diet (Teklad diet #2018) provided by the University of Ottawa ACVS, composed of 24% kcals protein, 18% kcals fat and 58% kcals carbohydrates, with 0.4% methionine and 1200mg/kg of choline[128]. In addition to weekly cleanings, body weight and overall physical condition were carefully monitored. After 20 weeks on the HFMCDD, diet-fed mice from E01 and E02 were returned to the standard chow diet for an additional 4 weeks.

2.5 Liver collection and histology

At endpoint, mice were euthanized by carbon dioxide inhalation at the University of Ottawa ACVS and the collected livers were perfused with 50mL of PBS through cardiac puncture. Liver sections were then fixed in 4% paraformaldehyde (Sigma-Aldrich, MO, USA) for 72 hours, then transferred to 70% ethanol. Samples were sent to the University of Ottawa Louise Pelletier

Histology Core Facility for paraffin embedding, sectioning, and staining. Liver sections were stained with Masson's Trichrome (MT) stain for visualization of fibrotic tissue, and with Hematoxylin and Eosin (H&E) for the visualization of ballooning, steatosis, and inflammation. Liver steatosis, inflammation, ballooning and fibrosis scores were determined, using the NAFLD activity (S0-3, I0-3, B0-2) and METAVIR scoring systems (F0-4), respectively, by an expert pathologist (Nour Histopathology Consultation Services, Ottawa, ON, Canada), blinded to the sample identities and treatments[129,130].

2.6 Blood collection, PBMC isolation, stimulation & culture

2.6a Blood collection, PBMC isolation, stimulation & culture in MASH patients

Frozen human PBMCs were thawed in a water bath and resuspended at $1x10^6$ cells/mL in warm complete RPMI medium (i.e. RPMI supplemented with 20% fetal calf serum and penicillin/streptomycin) and incubated at 37°C for 4-24h. $CD4^+$ T cells were isolated using the EasySep™ Human CD4 Positive Selection Kit II (Stemcell, BC, CAN). Samples were resuspended in sorting buffer (PBS with 2% FBS and 1mM EDTA) at $1x10^8$ cells/mL and transferred to 5mL polystyrene round-bottom tubes for magnetic separation. Cells were incubated for 3 minutes at room temperature with 50µL/mL of selection cocktail. Then, 50µL/mL of RapidSpheres™ were added for 3 minutes at room temperature before topping up the sample up to 2.5mL and placing them in the EasySep™ magnet for 3 minutes. The supernatant was discarded, and the desired cells remained in the tube. The last step was repeated two more times for a total of 9 minutes (3 x 3-minute separations)[131]. The isolated $CD4^+$ T cells (up to 96% purity) were washed with PBS, counted by trypan blue exclusion and resuspended at a density of $1x10^6$ cells/mL in 20% RPMI medium. The isolated cells were then plated at a density of $2x10^5$ cells/well with soluble Stimulant CD3/CD28/CD2 in ImmunoCult™ XF-T cells expansion medium (1:1 particle-

to-cell ratio, BioLegend, CA, USA) and cultured for 48 hours at 37°C before staining and analysis of cell functions.

2.6b Blood collection, PBMC isolation, stimulation & culture in C57BL/6 mice

At baseline and every subsequent 4 weeks, blood samples were collected from the lateral saphenous vein using heparin-containing Microvette CB300 tubes (Fisher Scientific, CA, USA), preventing coagulation. To remove red blood cell contamination and collect peripheral blood mononuclear cells (PBMCs), the blood was lysed with Hybri-Max^{TM} Red Blood Cell Lysing Buffer (Sigma-Aldrich, MO, USA) for 8 minutes. Pelleted cells were then washed with phosphate buffered saline (PBS), counted by trypan blue exclusion, and resuspended at a density of $1x10^6$ cells/mL in complete RPMI medium. A 96-well high-binding flat-bottom plate (Sarstedt, USA) was coated with anti-CD3 antibodies (5μg/mL in PBS, clone 145-2C11, BD Biosciences, CA, USA) for one hour at 37°C, then washed twice with PBS. Isolated PBMCs were then plated at a density of $2x10^5$ cells/well with soluble anti-CD28 antibodies (2μg/mL in complete RPMI medium, clone 37.51, BD Biosciences, CA, USA) and cultured for 48 hours at 37°C.

2.7 Flow cytometry

2.7a Extracellular & intracellular staining for $CD4^+$ T cell phenotyping in MASH patients

In the final five hours of cell culture, PBMCs were supplemented with protein transport inhibitors Brefeldin (GolgiPlug, BD Biosciences, CA, USA) and Monensin (GolgiStop, BD Biosciences, CA, USA). At the end of the 48-hour stimulation, cells were transferred to a 96-well v-bottom plate and washed with PBS. Dead cells were labelled with 100μL of Zombie Green (1:1000 dilution in PBS, Biolegend), and incubated for 20 minutes at room temperature. Then, 50μL of F_C block (clone Fc1.3216, BD Biosciences) was added to each well and incubated for an additional 20 minutes at room temperature to block non-specific antigen binding. To assess T cell

phenotypes, cells were stained with 100μL of cell surface mouse anti-human antibody cocktail containing BV711 CD4 (clone RPA-T4, BioLegend), APC-Cy7 CCR7 (clone G043H7, BioLegend), BV650 CD27 (clone M-T271, BioLegend) and Pacific Blue CD45RA (clone HI100, BioLegend). Following extracellular staining, cells were fixed using Cytofix/Cytoperm Fixation/Permeabilization kit (BD Biosciences, CA, USA) for 20 minutes at room temperature. Lastly, cells were stained with 100μL of PE-Cy7 IFN-γ (clone 4S.B3, BioLegend), BV785 IL-17 (clone BL168, BioLegend), APC Perforin (clone B-D48, BioLegend) and Alexa Fluor 700 TGF-β (clone 1018746, R&D Systems) cocktail for 30 minutes. T cell subsets were distinguished as follows: naïve (T_N, $CD45RA^+CCR7^+$), central memory ($T_{CM,}$ $CD45RA^-CCR7^+$) and effector/effector memory ($T_{E/EM}$, $CD45RA^-CCR7^-$). Samples were either compensated using cells and analyzed in relation to FMO controls on the Cytek Aurora at the University of Ottawa Flow Cytometry and Virometry Core Facility.

2.7b Extracellular & intracellular staining for $CD4^+$ T cell phenotyping in CCl_4-induced liver fibrosis mouse model

In the final five hours of cell culture, PBMCs were supplemented with protein transport inhibitors Brefeldin (GolgiPlug, BD Biosciences, CA, USA) and Monensin (GolgiStop, BD Biosciences, CA, USA). At the end of the 48-hour stimulation, cells were transferred to a 96-well v-bottom plate and washed with PBS. Dead cells were labelled with 100μL of Zombie Green (1:1000 dilution in PBS, Biolegend), and incubated for 20 minutes at room temperature. Then, 50μL of F_C block (clone 2.4G2, BD Biosciences) was added to each well and incubated for an additional 20 minutes at room temperature to block non-specific antigen binding. To assess T cell phenotypes, cells were stained with 50μL of cell surface rat anti-mouse antibody cocktail containing BV785 CD8 (clone 53.6-7, BioLegend), BV711 CD4 (clone GK1.5, BioLegend),

BV421 CD44 (clone IM7, BioLegend), PE CD62L (clone MEL-14, BioLegend) and BV650 CD19 (clone HIB19, BioLegend). Following extracellular staining, cells were fixed using Cytofix/Cytoperm Fixation/Permeabilization kit (BD Biosciences, CA, USA) for 20 minutes at room temperature. Lastly, cells were stained with 100μL of PE-Cy7 IFN-γ (clone 4S.B3, BioLegend), PE-CF594 GrzB (clone GB11, BD Biosciences and APC-Cy7 TNFα (clone Mab11, ThermoFisher) cocktail for 30 minutes. T cell subsets were distinguished as follows: naïve (T_N, $CD44^-CD62L^+$), central memory (T_{CM}, $CD44^+CD62L^+$) and effector/effector memory ($T_{E/EM}$, $CD44^+CD62L^-$). Samples were either compensated using cells and analyzed in relation to FMO or single controls on the Cytek Aurora at the University of Ottawa Flow Cytometry and Virometry Core Facility.

2.7c Extracellular & intracellular staining for $CD4^+$ T cell phenotyping in the HFMCDD-induced liver injury mouse model

In the final five hours of cell culture, PBMCs were supplemented with protein transport inhibitors Brefeldin (GolgiPlug, BD Biosciences, CA, USA) and Monensin (GolgiStop, BD Biosciences, CA, USA). At the end of the 48-hour stimulation, cells were transferred to a 96-well v-bottom plate and washed with PBS. Dead cells were labelled with 100μL of Zombie NIR (1:5000 dilution in PBS, Biolegend), and incubated for 20 minutes at room temperature. Then, 50μL of F_C block (clone 2.4G2, BD Biosciences) was added to each well and incubated for an additional 20 minutes at room temperature to block non-specific antigen binding. To assess T cell phenotypes, cells were stained with 50μL of cell surface rat anti-mouse antibody cocktail containing BV785 CD8 (clone 53.6-7, BioLegend), Alexa Fluor 700 CD4 (clone GK1.5, BioLegend), BV421 CD44 (clone IM7, BioLegend), PE CD62L (clone MEL-14, BioLegend) and PE-Cy5 CD19 (clone 6D5, BioLegend). Cells were then fixed using Cytofix/Cytoperm Fixation/Permeabilization kit (BD

Biosciences, CA, USA) for 20 minutes at room temperature. Lastly, cells were stained with 100μL of BV650 IFN-γ (clone XMG1.2, BioLegend), PE-CF594 GrzB (clone GB11, BD Biosciences and Alex Fluor 488 IL-17 (clone TC11-18H10.1, BioLegend) cocktail for 30 minutes. T cell subsets were distinguished as follows: naïve (T_N, $CD44^-CD62L^+$), central memory (T_{CM}, $CD44^+CD62L^+$) and effector/effector memory ($T_{E/EM}$, $CD44^+CD62L^-$). Samples were either compensated using cells and analyzed in relation to FMO or single controls on the Cytek Aurora at the University of Ottawa Flow Cytometry and Virometry Core Facility.

2.8 Triple Immunofluorescence (IF) staining & analysis

FFPE liver sections from the HFMCDD mouse model were sent to the Louise Pelletier Histology Core Facility to be stained for triple immunofluorescence (IF) staining. These tissue sections were first deparaffinized and pre-treated using heat mediated antigen retrieval with EDTA buffer (pH 9.0). Slides were then rehydrated in 1X TBST buffer and blocked for 30 minutes with Rodent Block M (BioCare RBM961G). Sections were then incubated with the following antibodies: rabbit anti-mouse CD4 (1:750 dilution, ab183685, Abcam), rat anti-mouse IFN-γ (1:20 dilution, #MM700, ThermoFisher), goat anti-mouse granzyme B (1:50 dilution, #PA5-47214, ThermoFisher), and rabbit anti-mouse CD8α (1:250 dilution, D4W2Z, Cell Signaling) overnight at 4℃. Sections were washed with 1X TBST, then incubated with the following secondary antibodies: donkey anti-rabbit IgG 647 (A-31573, ThermoFisher), donkey IgG anti-goat 568 (A-11057, ThermoFisher), and donkey anti-rat IgG 488 (A-21208, ThermoFisher) using a 1:500 dilution for 2 hours in the dark at room temperature. This was followed by incubation with a quencher (Vector TrueView Autofluorescence Quenching Kit #SP=8400, Vector Labs) to decrease autofluorescence. Sections were then washed, incubated with 5ug/mL of DAPI (ThermoScientific #62248) and cover slipped. These triple IF-stained livers were scanned by the

Louise Pelletier Histology Core Facility at 20x magnification using ZEISS Axioscan 8 Microscope Slide Scanner. Cell quantification was performed manually (T cells) and automatically (total cells) with the assistance of QuPath 0.5.1 open-source software (Refer to Fig 1) to choose 15 randomized tissue regions/sections and all data were graphed using GraphPad Prism 10.0 software.

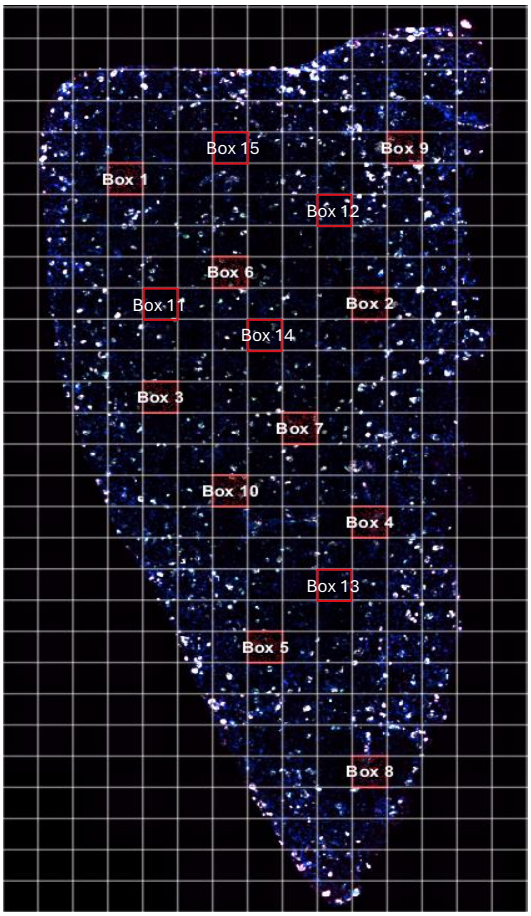

Figure 1: Randomized tissue region selection by QuPath software to facilitate automated and manual cell counting of triple IF-stained murine liver tissue sections.

2.9 Data analysis & statistics

Flow cytometry experiments were completed on the Cytek Aurora, and compensation was performed in SpectroFlo® software. Data were analyzed using FlowJo 10.8.2 software. Triple immunofluorescence images were obtained by the Louise Pelletier Histology Core Facility at 20x magnification using ZEISS Axioscan 8 Microscope Slide Scanner. All graphs and statistics were generated using GraphPad Prism 10.0 software. Data are presented as means ± standard deviation

(SD), and statistical analyses were completed using unpaired one-tailed Student's *t*-test and two-way ANOVA, where statistical significance was considered as $p \leq 0.05$.

CHAPTER 3: RESULTS

3.1 Human MASH with minimal or advanced liver fibrosis

3.1.1. $CD4^+$ T cell function in MASH

In MASLD, the dysregulation of $CD4^+$ T cell function has proven to play an important role in the progression of the disease, specifically aggravating liver inflammation and fibrosis in MASH[77,132]. In prior studies, an increase in cytokines, IFN-γ, TNF-α and IL-17, as produced by $CD4^+$ T cells, was found in peripheral blood of MASLD patients, as well as in MASH patients.[72] In this study, blood samples were collected from healthy donors, as well as MASH patients with minimal or advanced liver fibrosis. Flow cytometry analysis of isolated bulk $CD4^+$ T cells stimulated with anti-CD3/CD28 antibodies (Fig 2A-E) was conducted. This study revealed significant increases in the proportions of IFN-γ^+ and TGF-β^+CD4^+ T cells in MASH patients with advanced liver fibrosis (F4) in comparison to those with minimal fibrosis (F0-1) and healthy patients (Fig 2F-G). No significant differences were observed in the proportions of IL-17^+CD4^+ T cells (Fig 2H) and a significant decrease in the proportions of perforin$^+CD4^+$ T cells were observed in MASH patients with advanced liver fibrosis compared to healthy controls (Fig 2I). In keeping with previous studies in the Crawley lab, T cell subsets were evaluated (Fig 3B). No differences were observed in IFN-γ^+CD4^+ T cell subsets, however, there was an increase in the proportions in TGF-β^+ naïve $CD4^+$ T (T_N) cells in MASH patients with advanced liver fibrosis (F4) in comparison to the other two study groups (Fig 3C).

Studies have shown that males tend to exhibit more severe steatosis/steatohepatitis, more advanced fibrosis, elevated pro-inflammatory cytokine levels, higher liver tumour incidence and increased overall mortality[8]. Unfortunately, in this study, we were unable to perform sex difference analyses in regard to the proportions of IFN-γ^+, TGF-β^+, IL-17^+ or perforin$^+CD4^+$ T cells in

controls, MASH with minimal liver fibrosis and MASH with advanced liver fibrosis (Fig 4A-D), due to small sample size and age differences. Ongoing studies in the Crawley lab with additional MASH patients from both sexes are taking place to make conclusive statements on sex effects.

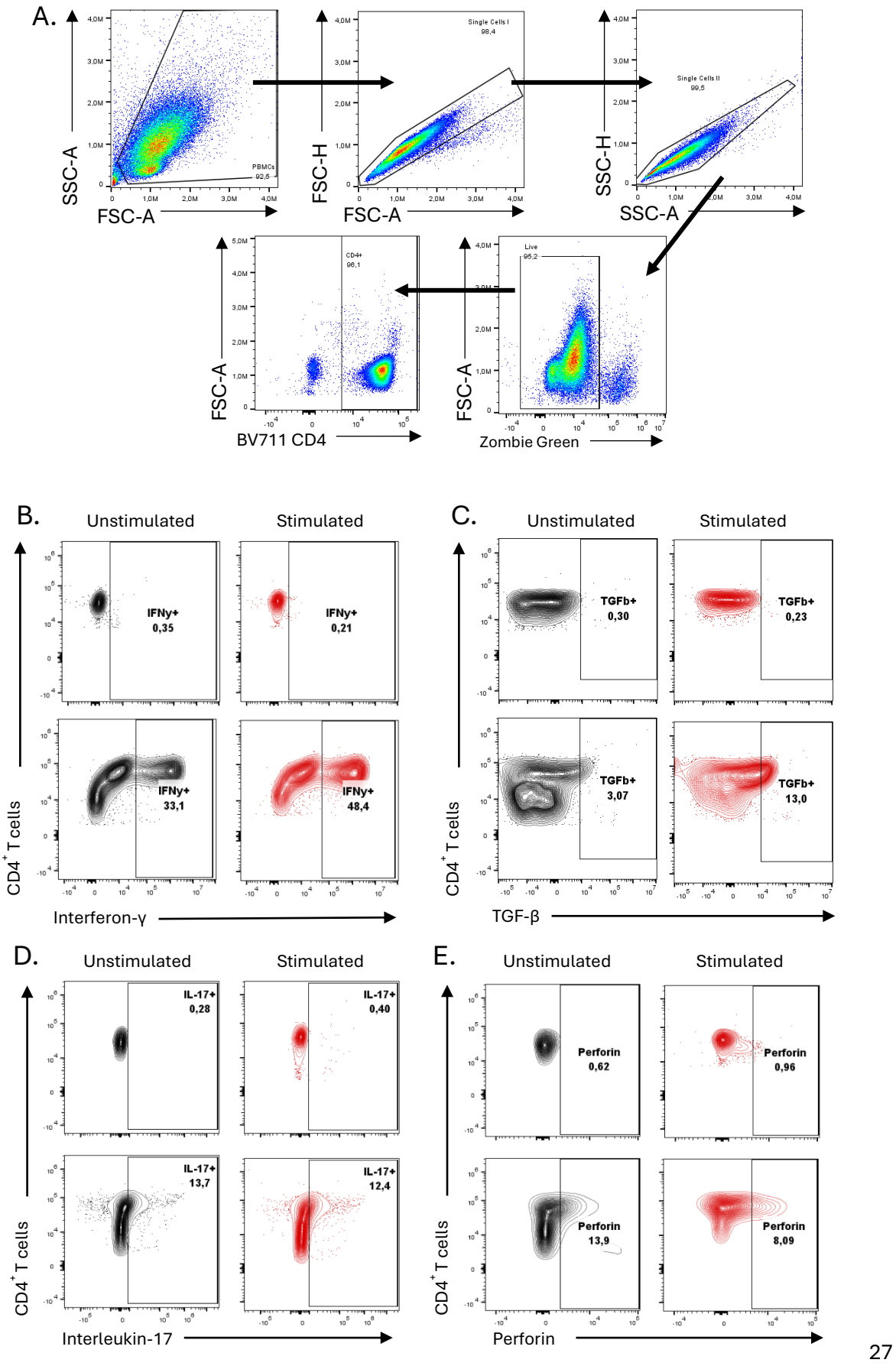
A.
SSC-A
FSC-A
PBMCs
92,5
FSC-H
FSC-A
Single Cells I
98,4
SSC-H
SSC-A
Single Cells II
99,5
FSC-A
BV711 CD4
CD4+
96,1
FSC-A
Zombie Green
Live
95,2
B.
Unstimulated
Stimulated
IFNγ+
0,35
IFNγ+
0,21
IFNγ+
33,1
IFNγ+
48,4
CD4+ T cells
Interferon-γ
C.
Unstimulated
Stimulated
TGFb+
0,30
TGFb+
0,23
TGFb+
3,07
TGFb+
13,0
CD4+ T cells
TGF-β
D.
Unstimulated
Stimulated
IL-17+
0,28
IL-17+
0,40
IL-17+
13,7
IL-17+
12,4
CD4+ T cells
Interleukin-17
E.
Unstimulated
Stimulated
Perforin
0,62
Perforin
0,96
Perforin
13,9
Perforin
8,09
CD4+ T cells
Perforin

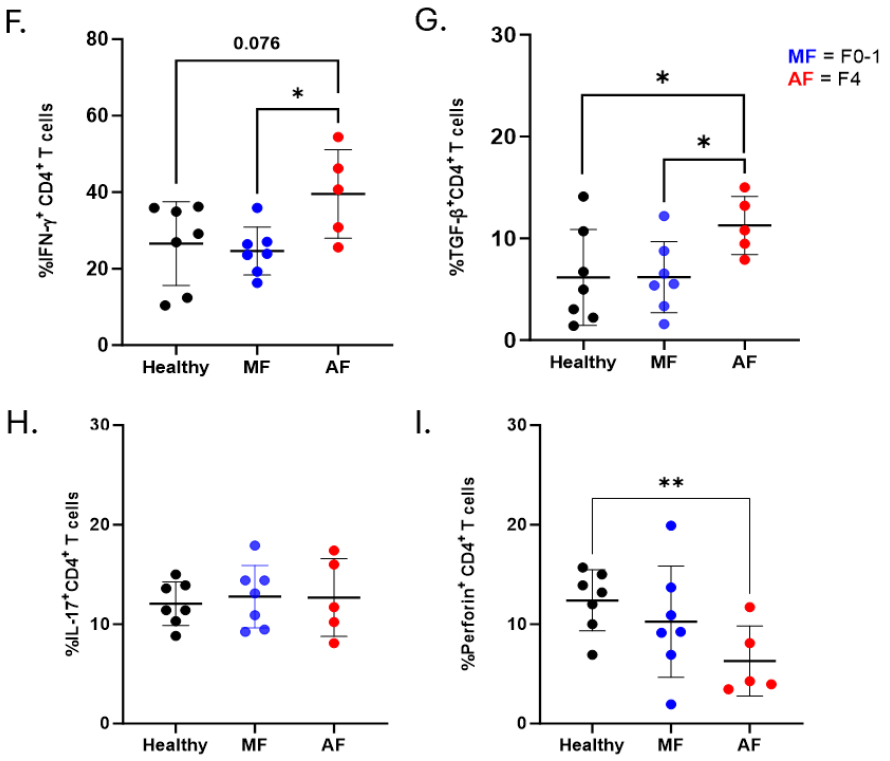

Figure 2: IFN-γ and TGF-β expression is elevated in MASH patients with advanced liver fibrosis. Blood samples were collected from donors, $CD4^+$ T cells were isolated from PBMCs, then stimulated with anti-CD3 and anti-CD28 beads for 48h. Representative flow cytometry gating strategy for **A)** PBMCs, single cells, live cells and $CD4^+$ cells. Representative responses of $CD4^+$ T function, demonstrating the expression of **B)** IFN-γ, **C)** TGF-β, **D)** IL-17, and **E)** perforin using unstimulated samples to set respective gates as shown. Increase in the proportions of **F)** IFN-γ^+CD4^+ T cells and **G)** TGF-β^+CD4^+ T cells in MASLD with advanced liver fibrosis (F4) in comparison to health and MASH with minimal liver fibrosis (F0-1). No difference in **H)** IL-17^+CD4^+ T cells between groups. Decrease in the proportions of **I)** perforin$^+CD4^+$ T cells in MASH with advanced liver fibrosis (F4) in comparison to health. Data are presented as group means ±SD and statistically significant differences were determined using a one-tailed unpaired Student's t-test (*$p \leq 0.05$,**$p \leq 0.01$).

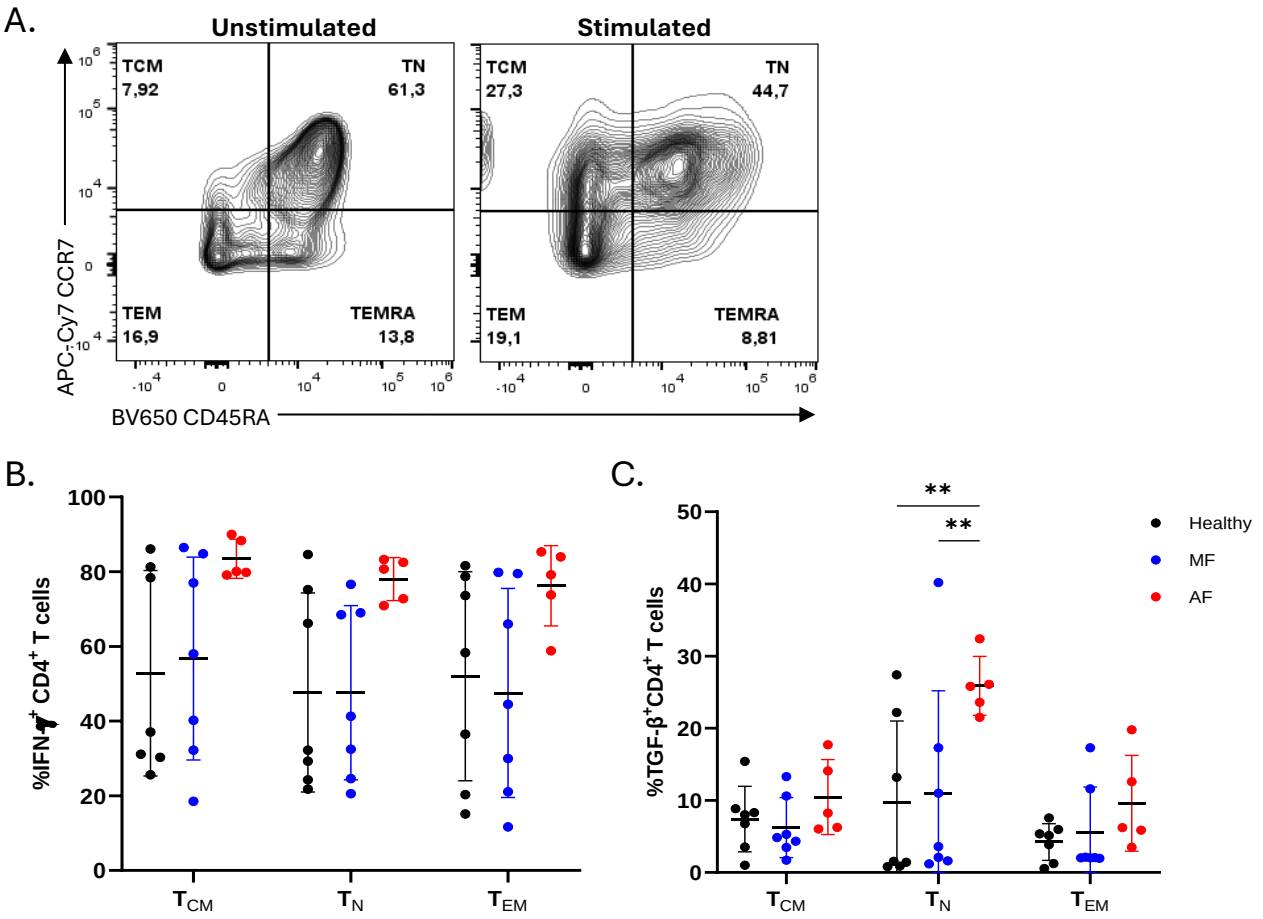

Figure 3: Increased proportions of TGF-β$^+$naïve CD4$^+$ T cells in MASH patients with advanced liver fibrosis. Blood samples were collected from donors, and CD4$^+$ T cells were isolated from PBMCs, then stimulated with anti-CD3 and anti-CD28 beads for 48h. Representative gating strategy of **A)** CD4$^+$ T cell subsets using unstimulated samples to set respective gates as shown. Using CD45RA and CCR7 markers, naïve (CD45RA$^+$CCR7$^+$, T_N), central memory (CD45RA$^-$CCR7$^+$, T_{CM}), effector memory (CD45RA$^-$CCR7$^-$, T_{EM}) and terminally differentiated effector memory T cells-expressing CD45RA (CD45RA$^+$, CCR7$^-$, T_{EMRA}) CD4$^+$ T cells were distinguished. No differences observed in the proportions of **B)** IFN-γ$^+$CD4$^+$ T cell subsets, although, increased proportions of **C)** TGF-β$^+$ T_N CD4$^+$ T cells were observed in MASH patients with advanced liver fibrosis compared to two other study groups. Data are presented as group means ±SD and statistically significant differences were determined using a one-tailed unpaired Student's t-test (**p≤0.01).

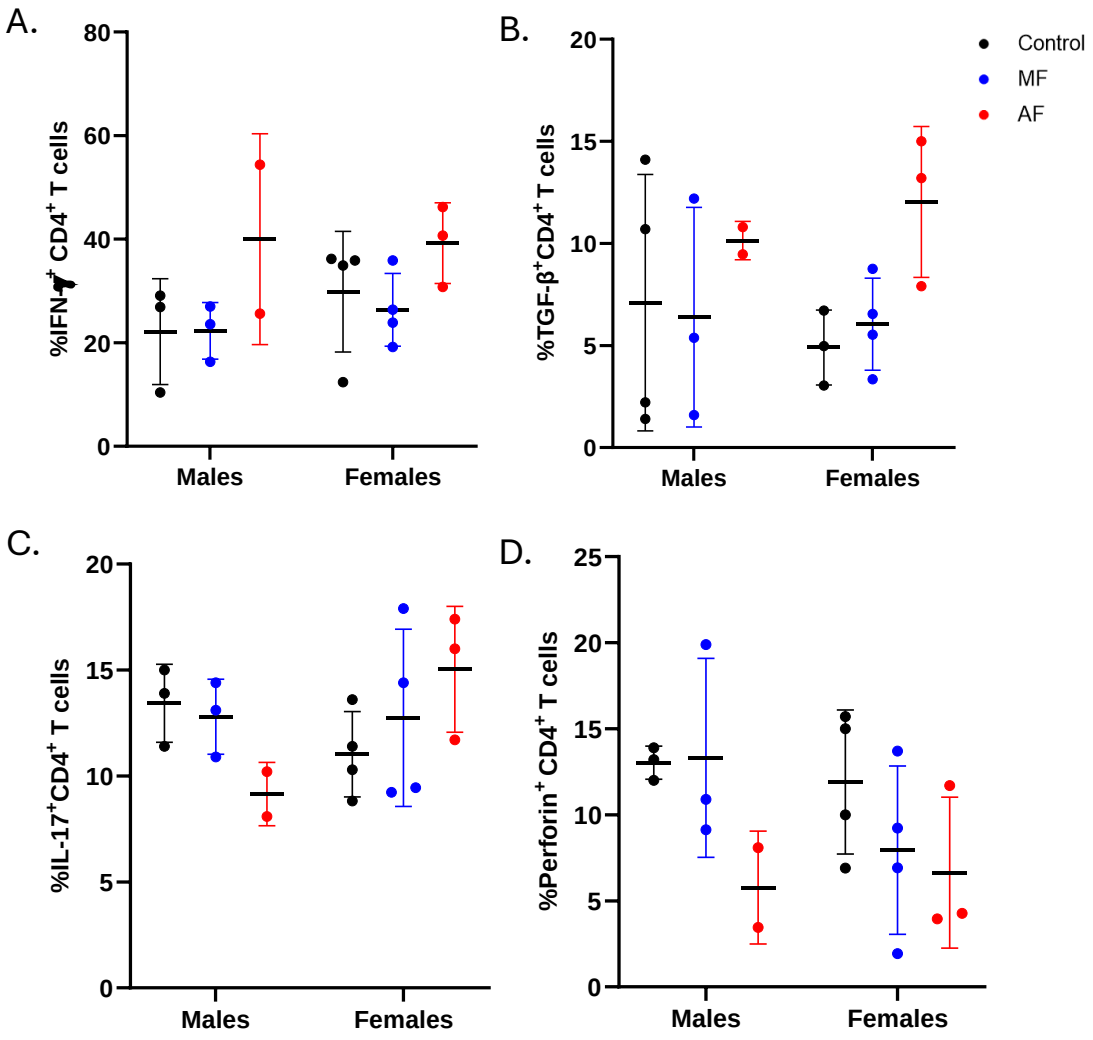

Figure 4: No sex differences between healthy, MASH patients with minimal or advanced liver fibrosis. Blood samples were collected from donors, and $CD4^+$ T cells were isolated from PBMCs, then stimulated with anti-CD3 and anti-CD28 beads for 48h. No sex differences observed in **A)** IFN-γ^+, **B)** TGF-β^+, **C)** IL-17^+ or **D)** perforin$^+$$CD4^+$ T cells. Data are presented as group means ±SD and a one-tailed unpaired Student's t-test was performed, although no statistically significant differences were observed.

3.2 Carbon tetrachloride model: hepatotoxin-induced liver fibrosis

3.2.1. CCl_4-induced liver fibrosis

In these experiments, 11-week-old C57BL/6 mice were injected twice a week intraperitoneally (i.p.) with 1.0ml/kg of 99% CCl_4 diluted to 50% in olive oil for 14-21 weeks, while control mice were injected with only olive oil (Fig 5A). To mimic liver injury observed during chronic HCV infection, CCl_4 is administered at regular intervals causing progressive liver damage and fibrosis, by impairing the plasma, lysosomal and mitochondrial membrane permeability of hepatocytes, thus promoting the formation of free radicals, causing centrilobular necrosis.[119] At endpoint, livers were collected, formalin-fixed, paraffin-embedded and stained with MT for pathology scoring. This dye imparts a blue colour to collagen (fibrotic scar tissue) while staining background hepatocytes red, thus allowing for histological evaluation of liver fibrosis[133]. Previous studies in the Crawley Lab have demonstrated that after only 12 weeks of CCl_4 administration, advanced liver fibrosis can be observed in treated mice in comparison to controls[100].

In E09, consisting of 22 mice (9 ctrl, 13 CCl_4), after 21 weeks of CCl_4 administration, mice were euthanized, and livers were collected and stained for histology (Fig 5B-C). In this study group, CCl_4-treated mice had significantly elevated liver fibrosis scores (mean F3±SD) in comparison to controls (mean F2±SD) (Fig 5D). When separating these findings by sex, all CCl_4-treated males developed advanced liver fibrosis (F3), which is statistically significant in comparison to controls (Fig 5E). In CCl_4-treated females, due to an uncharacteristically large variability in fibrosis scores for this model, there was no statistically significant difference from controls (Fig 5F).

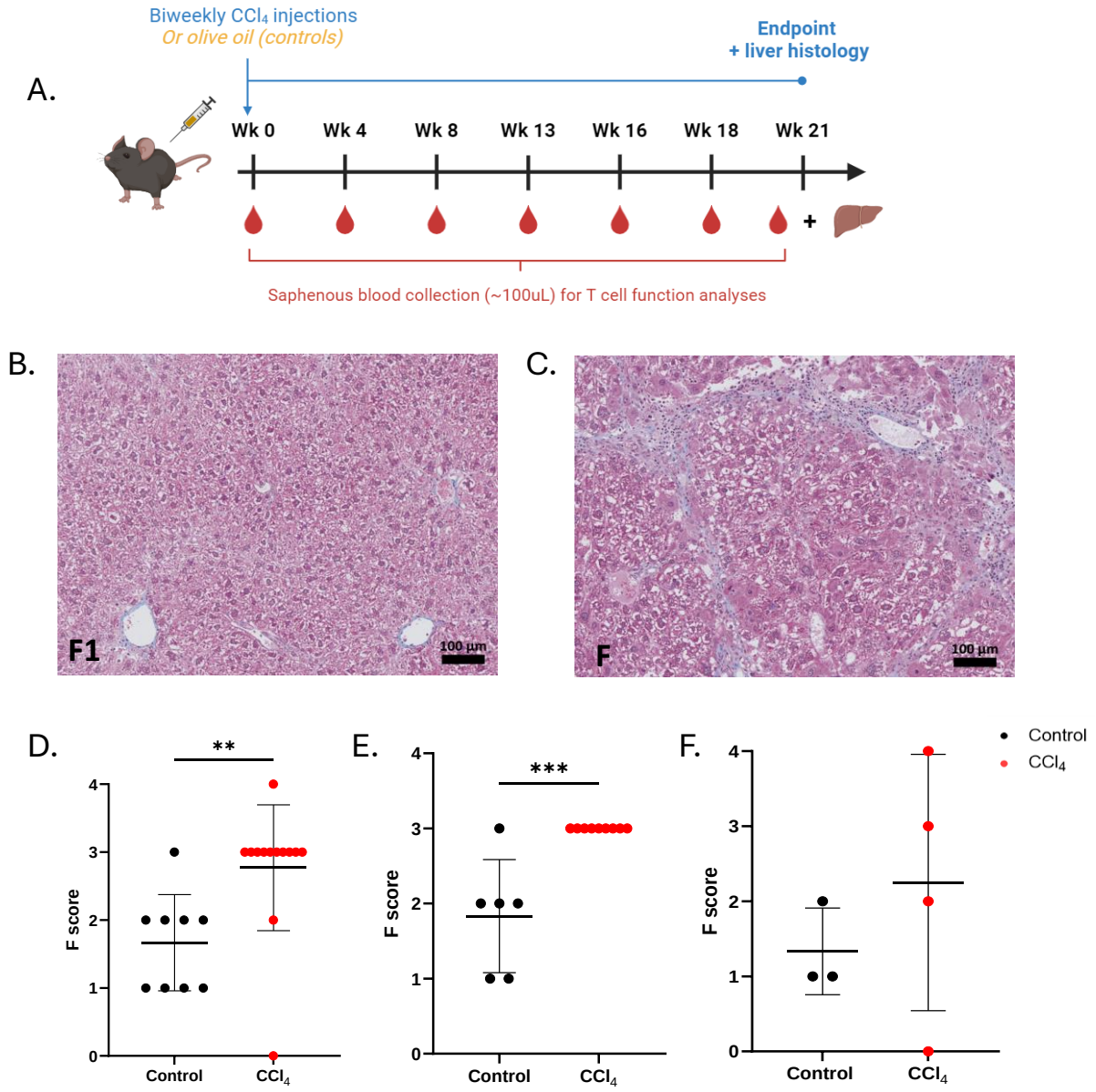

Figure 5: CCl_4 induces advanced liver fibrosis after 14-21 weeks of treatment. A) Schematic of experimental design. Mice were injected i.p. with CCl_4 twice weekly for 21 weeks. Saphenous blood was collected, PBMCs were isolated, then stimulated with anti-CD3/CD28 for 48 hours. At end of treatment, mice were euthanized, and livers were collected, formalin-fixed and paraffin-embedded. Representative liver histology images for **B)** chow mice (F1) and **C)** CCl_4-treated mice (F3) at end of treatment. Increased liver fibrosis scores in CCl_4-treated mice from **D)** the entire cohort (n= 15M, 7F), in **E)** males and **F)** females, compared to controls after 21 weeks. Data are presented as group means ±SD and statistically significant differences were determined using a one-tailed unpaired Student's t-test (**p≤0.01, ***p≤0.001). Scale bar = 100 µM.

3.2.2. $CD4^+$ T cell function in CCl_4-treated mice

At baseline and at 4-week intervals, saphenous blood samples were collected and PBMCs were isolated from the CCl_4-treated and control mice. To assess T cell phenotypes, PBMCs were labelled with a variety of fluorochrome-conjugated anti-mouse antibodies (refer to section 2.8). In the Crawley lab, this well established hepatotoxin-induced liver fibrosis murine model has proven to cause generalized $CD8^+$ T cell hyperfunction, characterized by increases in the proportions of IFN-γ^+ and $GrzB^+CD8^+$ T cells in treated mice compared to controls[100]. In a previous CCl_4 study, preliminary data suggested that a significant increase in the proportions of $GrzB^+CD4^+$ T cells was found in CCl_4-treated mice *(Crawley, unpublished*).

In two independent CCl_4 studies, flow cytometry analysis of bulk $CD4^+$ T cells (Fig 6A-D) and $CD4^+$ T cell subsets (Fig 6E) were conducted. In **E09**, conducted in collaboration with PhD candidate Jiafeng Li, transient increases in the proportions of $GrzB^+$ and TNF-α^+CD4^+ T cells were observed after 18 weeks of treatment (Fig 6F-G). No differences were observed in IFN-γ^+ bulk $CD4^+$ T cells or subsets throughout the study (Fig 6H). There were, also, transient increases in the proportions of $GrzB^+$ T_{CM} and $T_{E/EM}$ $CD4^+$ T cells at week 18 (Fig 6I). No differences were observed in any subsets for IFN-γ^+ or TNF-α^+CD4^+ T cells. In **E10**, conducted in collaboration with PhD candidate David Lawton, no significant differences were observed in IFN-γ^+, $GrzB^+$ and TNF-α^+CD4^+ T cells after 14 weeks of treatment (Fig 7A-C). Unlike the first 5 cohorts previously studied in the CCl_4 model, $CD8^+$ T cell hyperfunction was not replicated here, and evidence of $CD4^+$ T cell hyperfunction was either transient or absent.

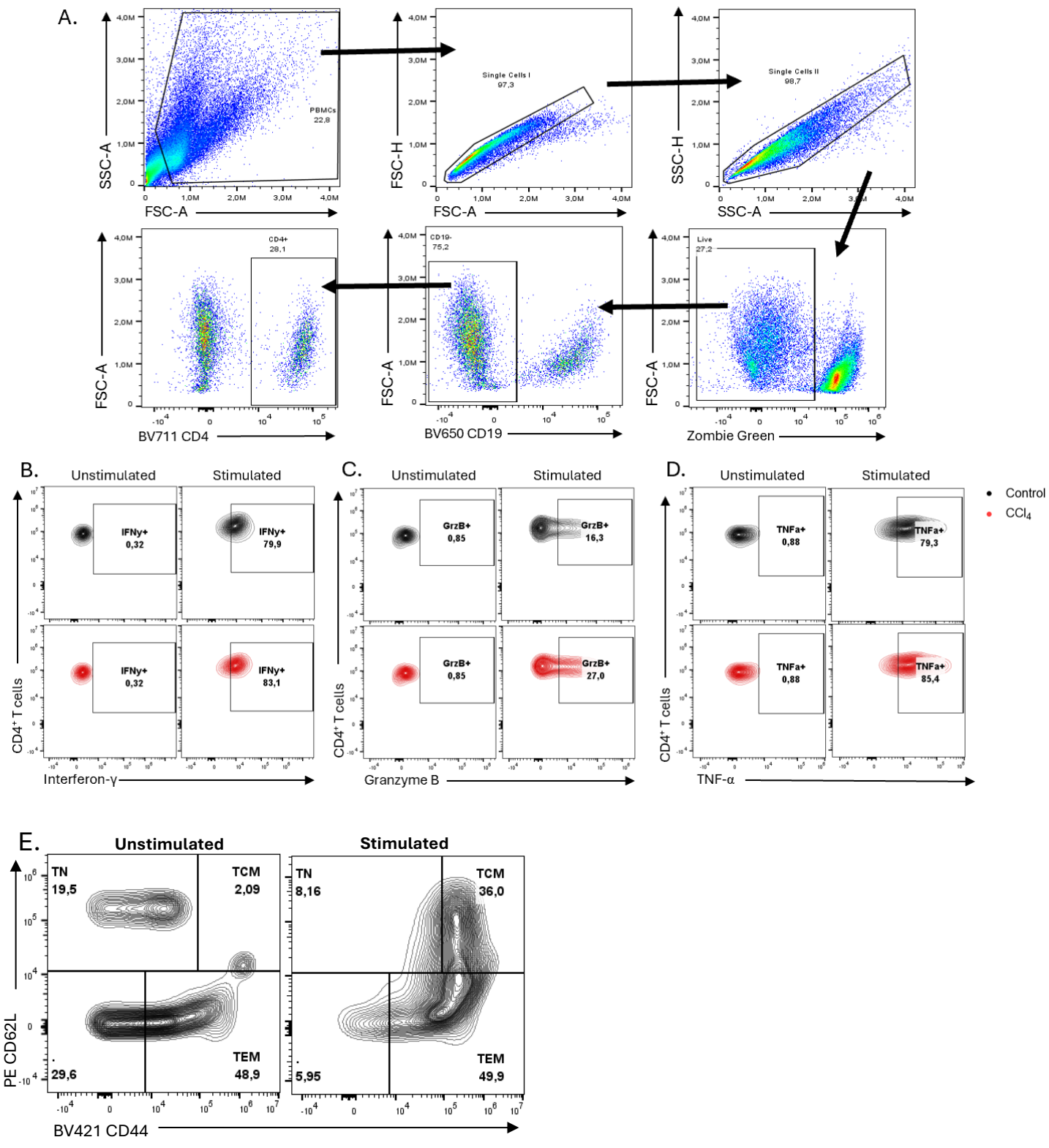
A.
SSC-A
FSC-A
PBMCs
22,8
FSC-H
Single Cells I
97,3
SSC-H
Single Cells II
98,7
CD4+
28,1
BV711 CD4
CD19-
75,2
BV650 CD19
Live
27,2
Zombie Green
B.
Unstimulated
Stimulated
IFNγ+
0,32
IFNγ+
79,9
IFNγ+
0,32
IFNγ+
83,1
CD4+ T cells
Interferon-γ
C.
Unstimulated
Stimulated
GrzB+
0,85
GrzB+
16,3
GrzB+
0,85
GrzB+
27,0
Granzyme B
D.
Unstimulated
Stimulated
TNFa+
0,88
TNFa+
79,3
TNFa+
0,88
TNFa+
85,4
TNF-α
Control
CCl4
E.
Unstimulated
Stimulated
TN
19,5
TCM
2,09
TEM
48,9
29,6
TN
8,16
TCM
36,0
TEM
49,9
5,95
PE CD62L
BV421 CD44

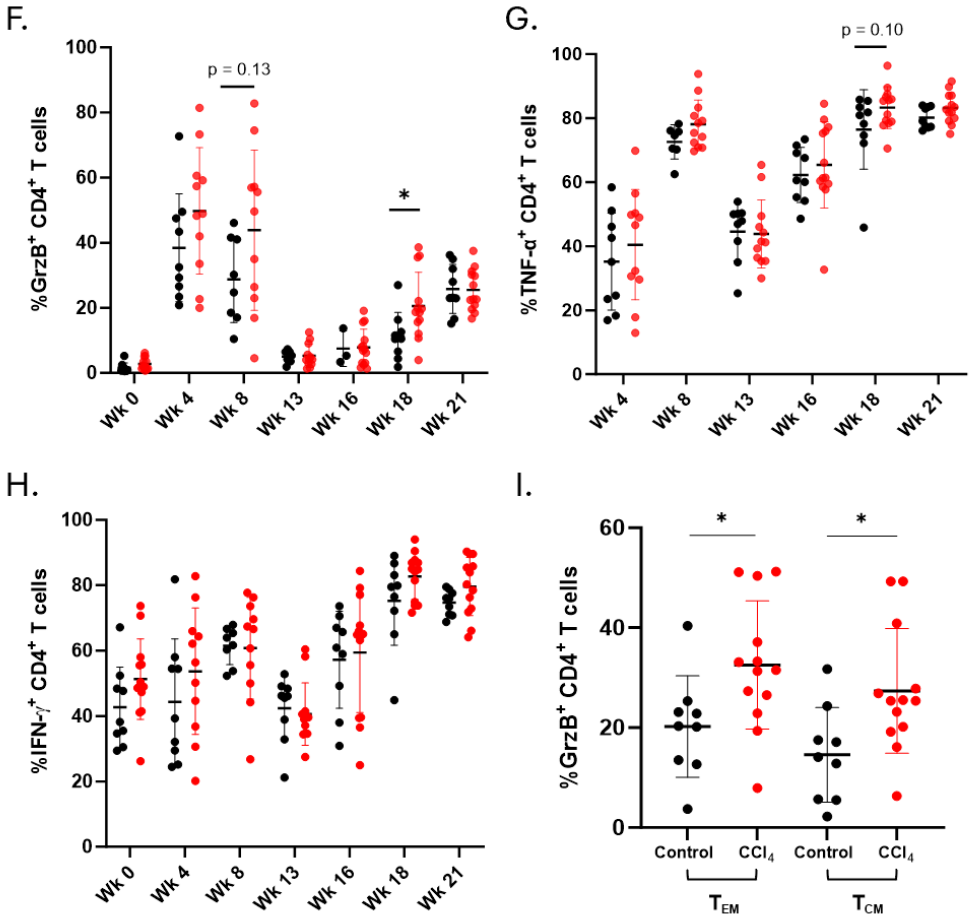

Figure 6: Transient increases in the proportions of GrzB$^+$ and TNF-α$^+$CD4$^+$ T cells after 18 weeks of CCl_4 treatment. Mice were injected i.p. with CCl_4 twice weekly for 21 weeks. Saphenous blood was collected, PBMCs were isolated, then stimulated with anti-CD3/CD28 for 48 hours. The representative flow cytometry gating strategy for **A)** PBMCs, single cells, live cells and CD19$^-$CD4$^+$ cells. Representative responses of CD4$^+$ T cell function, demonstrating the expression **B)** IFN-γ, **C)** GrzB, **D)** TNF-α and **E)** T_N, T_{CM} and $T_{E/EM}$ subsets using unstimulated samples to set respective gates as shown. **F)** No difference in proportions of IFN-γ^+CD4$^+$ T cells. **G)** Transient increased proportions of GrzB$^+$CD4$^+$ T cells in CCl_4-treated mice after 18 weeks of CCl_4 treatment. **H)** Trending increase in proportions of TNF-α$^+$CD4$^+$ T cells at week 8 of CCl_4 treatment. We observed increases in the proportions of **I)** GrzB$^+$ T_{CM} and $T_{E/EM}$ CD4$^+$ T cells after 18 weeks of treatment. Data are presented as group means ±SD and statistically significant differences were determined using a one-tailed unpaired Student's t-test (*p≤0.05).

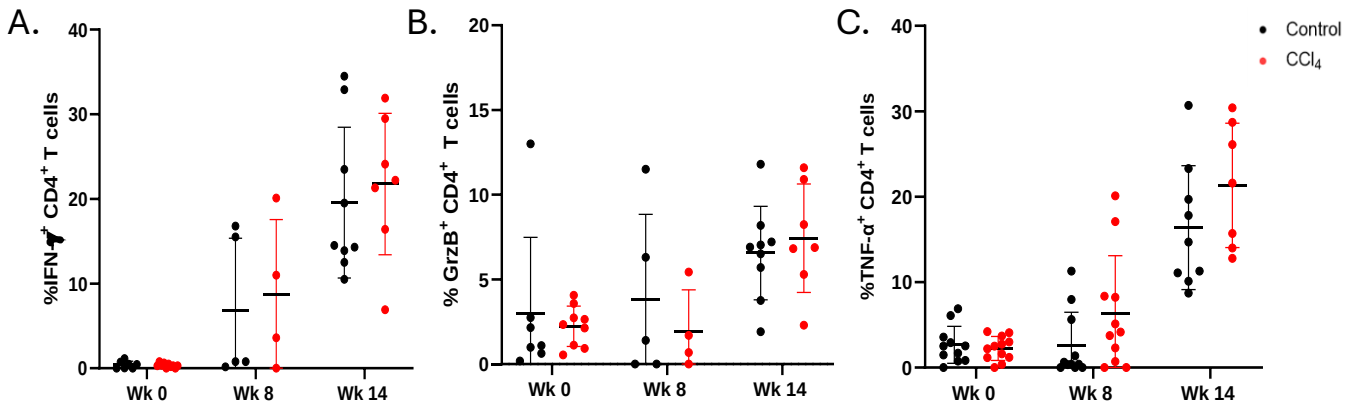

Figure 7: No CD4$^+$ T cell hyperfunction observed after 14 weeks of CCl_4 treatment. After 14 weeks, blood PBMCs were collected and stimulated with anti-CD3/CD28 for 48 hours. No difference in proportions of **A)** IFN-γ^+, **B)** GrzB$^+$ or **C)** TNF-α^+CD4$^+$ T cells observed after 14 weeks of CCl_4 treatment. Data are presented as group means ±SD and a one-tailed unpaired Student's t-test was performed but no significant differences were found.

3.3 HFMCDD model: diet-induced liver injury

3.3.1. HFMCDD-induced liver injury

a. Liver injury at peak HFMCDD treatment

In collaboration with MSc graduate Katrina Jorritsma, three independent studies were conducted, during which C57BL/6 mice fed a high-fat methionine and choline deficient diet (HFMCDD) *ad* libitum for a duration of 16-21 weeks (Fig 8A). The diet consists of 60% of kcal from fat, 0.1% methionine and 0.0% choline, and is used to replicate MASLD histopathology, while controls were fed a standard chow diet. The high-fat component promotes weight gain and with time, liver damage, while the methionine and choline deficiencies impair metabolic pathways, thus promoting weight loss and liver fibrosis. Signs of liver steatosis and fibrosis can be observed as early as 3 and 6 weeks, respectively, after the start of the HFMCDD diet in C57BL/6 mice[134,135]. At peak treatment, a subset of animals was euthanized for histology, where liver sections were stained with MT to visualize fibrotic tissue, and H&E to visualize steatosis as well as inflammation.

In three independent HFMCDD studies (E01, E02 and E03), liver tissue sections were sectioned and stained for analysis. In **E01**, consisting of 21 males (9 ctrl, 12 diet), after 20 weeks of diet feeding, the majority of HFMCDD-fed mice developed advanced liver fibrosis (mean F4 ±SD) and advanced liver steatosis in comparison to controls (F0, S0) (Fig 8B-F). In **E02**, consisting of 19 females (7 ctrl, 12 diet), after 20 weeks of diet feeding, HFMCDD-fed mice developed moderate-to-advanced liver fibrosis (F2-3) and advanced liver steatosis (S3), while the livers of controls remained unaffected (F0, S0) (Fig 9A-E). This demonstrates sex differences, where females do not develop fibrosis as far advanced as males. In **E03**, consisting of 12 males (6 ctrl, 6 diet) and 12 females (7 ctrl, 5 diet), after 16 weeks of diet feeding, HFMCDD-fed mice developed moderate-to-advanced liver fibrosis (F2-4) and advanced liver steatosis (S3), compared to their

controls (F0-1, S0) (Fig 10A). These statistically significant differences remained once stratified by sex (Fig 10B). In human MASLD and MASH, similar findings have been observed, where males tend to develop more severe liver injury[7].

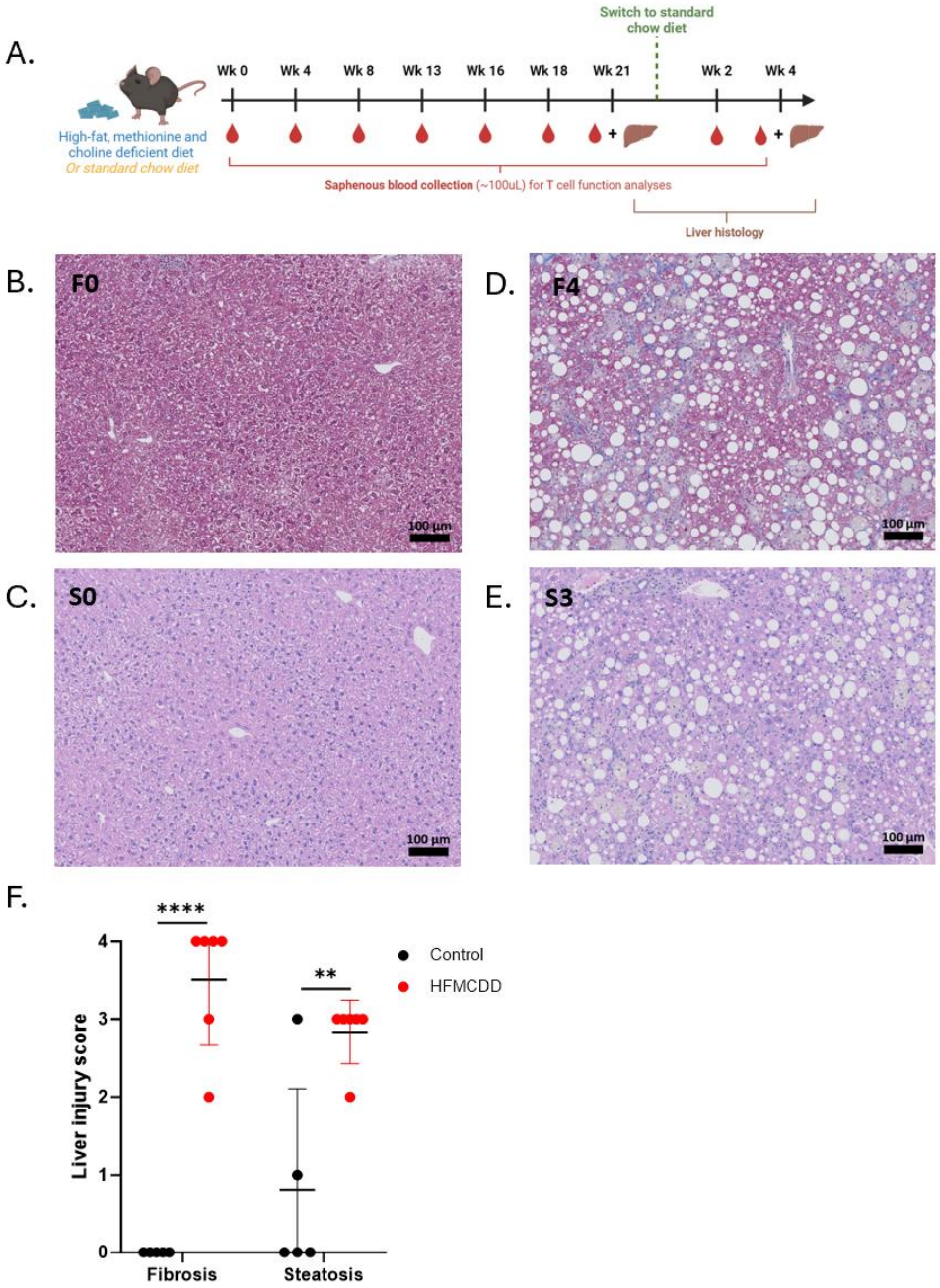

Figure 8: Twenty weeks of HFMCDD feeding induces advanced liver fibrosis and steatosis in males. A) Schematic of experimental design of the HFMCDD murine mode. Mice were fed a HFMCDD *ad libitum* for 20 weeks, while control mice were fed a standard chow diet. At peak treatment, a subset of animals was euthanized, and liver sections were collected for histology. Representative MT and H&E liver histology images for **B-C)** control (F0, S0) and **D-E)** HFMCDD-fed mouse after 20 weeks of diet feeding (F4, S3). Higher liver injury scores in **F)** HFMCDD-fed males, compared to controls. Data are presented as group means ±SD and statistically significant differences were determined using a one-tailed unpaired Student's t-test (**p≤0.01,****p≤0.0001). Scale bar = 100 µM.

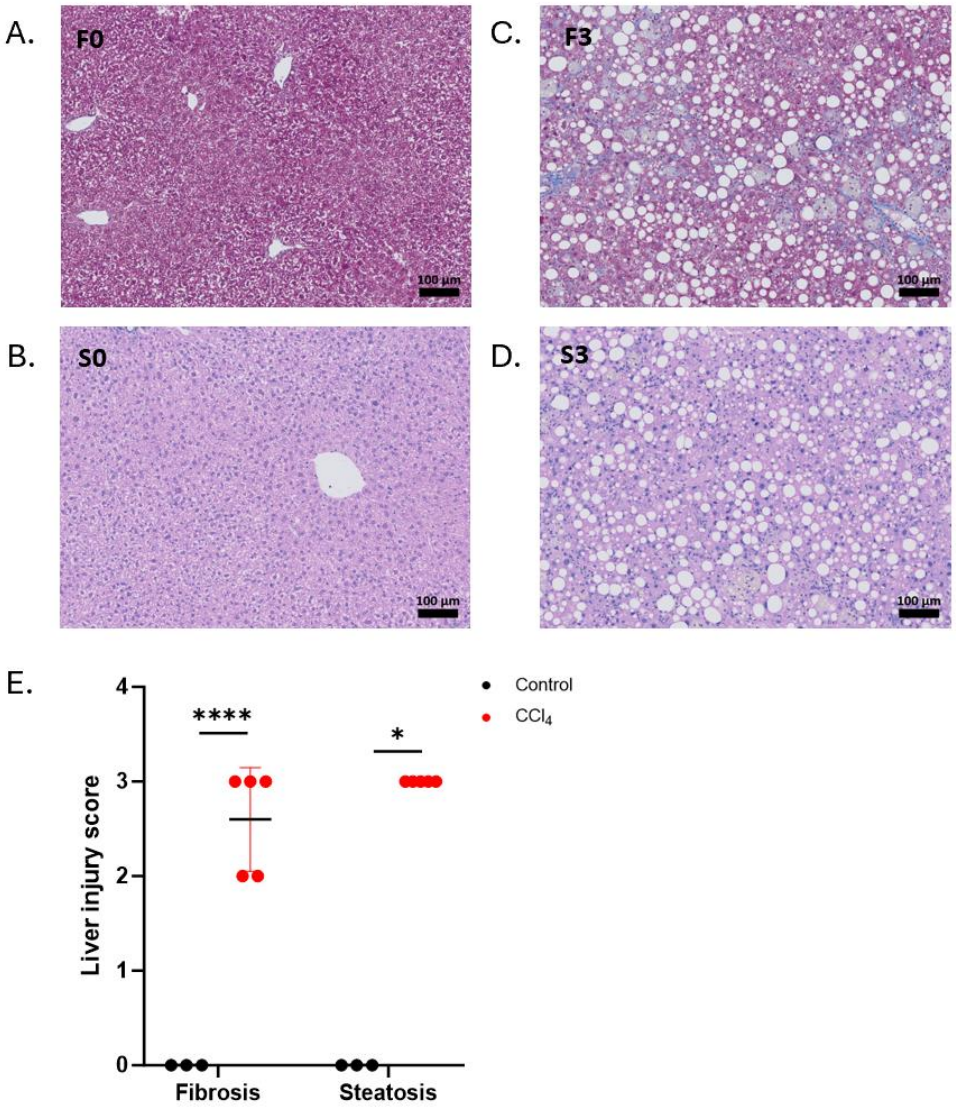

Figure 9: Twenty weeks of HFMCDD feeding induces advanced liver fibrosis and steatosis in females. Mice were fed a HFMCDD *ad libitum* for 20 weeks, while control mice were fed a standard chow diet. At peak treatment, a subset of animals was euthanized, and liver sections were collected for histology. Representative MT and H&E liver histology images for **A-B)** control (F0, S0) and **C-D)** HFMCDD-fed mouse after 20 weeks of diet feeding (F3, S3). Higher liver injury scores in **E)** HFMCDD-fed females, compared to controls. Data are presented as group means ±SD and statistically significant differences were determined using a one-tailed unpaired Student's t-test (*$p \leq 0.05$,****$p \leq 0.0001$). Scale bar = 100 µM.

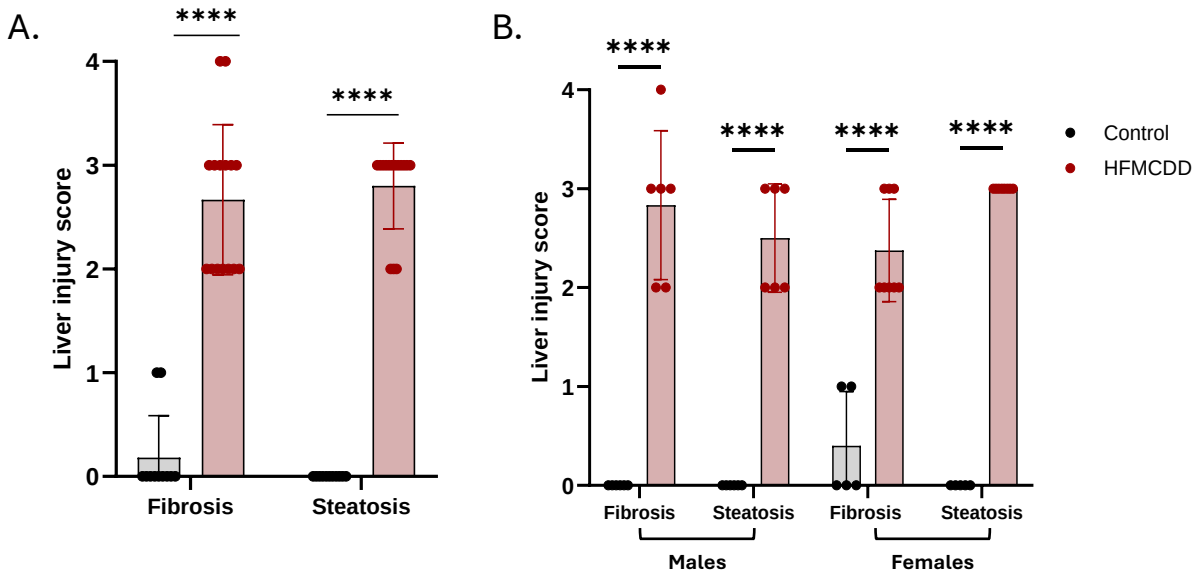

Figure 10: Sixteen weeks of HFMCDD feeding induces advanced liver fibrosis and steatosis. Mice were fed a HFMCDD ad libitum for 16 weeks, while control mice were fed a standard chow diet. At peak treatment, a subset of animals was euthanized, and liver sections were collected for histology. Higher liver injury scores in HFMCDD-fed mice from **A)** the entire cohort (n= 12F, 12M), and when **B)** separated by sex. Data are presented as group means ±SD and statistically significant differences were determined using a one-tailed unpaired Student's t-test (****$p \leq 0.0001$). Scale bar = 100 µM.

b. Liver injury regression 4 weeks post-HFMCDD cessation

After being fed an HFMCDD for 20 weeks, mice were returned to the standard chow diet for an additional 4 weeks to study liver injury regression. Animals were euthanized, and liver sections were then preserved and stained with MT to visualize fibrotic tissue, and H&E to visualize steatosis and inflammation. Interestingly, after the 4-week regression period, liver fibrosis scores in HFMCDD-fed males reduced from advanced liver fibrosis (F4) to moderate liver fibrosis (F3), while in HFMCDD-fed females remained unchanged at moderate liver fibrosis (F2-3). Liver steatosis scores in HFMCDD-fed males reduced to control levels (S0-2), while in HFMCDD-fed females, steatosis completely resolved (Fig 11A-F).

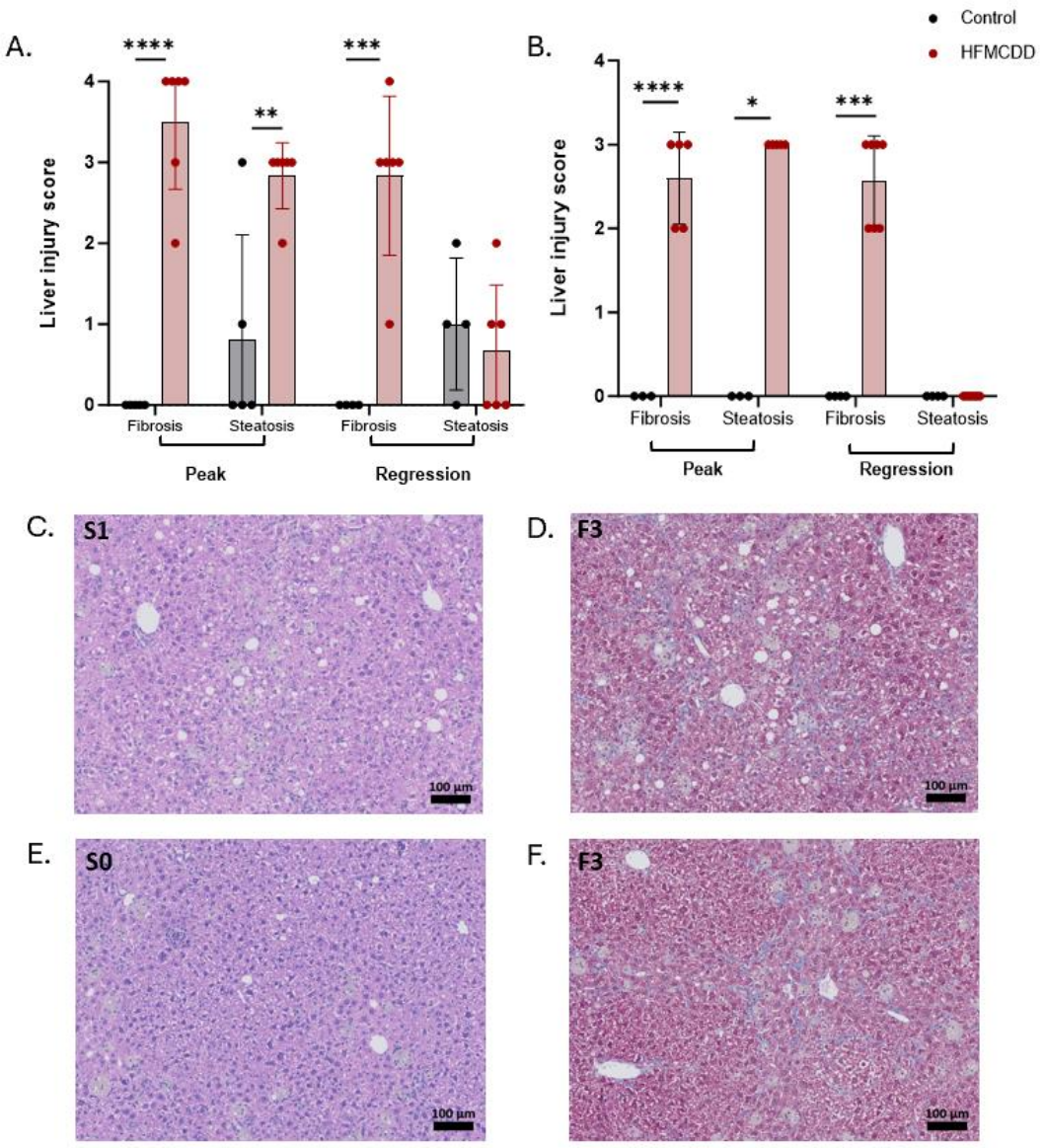

Figure 11: Steatosis reversal 4 weeks after HFMCDD cessation. Mice were fed a HFMCDD ad libitum for 20 weeks, while control mice were fed a standard chow diet. After this time period, mice returned to the standard chow diet. Subsets of animals were euthanized after the initial 20 weeks and 4 weeks post-HFMCDD cessation, and liver sections were collected for histology. HFMCDD-induced liver injury and regression of organ damage in **A)** males and **B)** females. Representative H&E and MT histology images for **C-D)** HFMCDD-fed male and **E-F)** female after undergoing 4 weeks of HFMCDD cessation. Data are presented as group means ±SD and statistically significant differences were determined using a one-tailed unpaired Student's t-test (*p≤0.05, **p≤0.01, ***p≤0.001, ****p≤0.0001). Scale bar = 100 µM.

3.3.2. $CD4^+$ T cell function in HFMCDD-fed males

a. $CD4^+$ T cell function at peak HFMCDD treatment

At baseline and at intervals of 4 weeks, PBMCs were isolated from blood samples collected from HFMCDD-fed and control mice, then stained with a variety of flow cytometry antibodies (refer to section 2.9). Concurrent $CD8^+$ T cell studies in the Crawley Lab, demonstrated $CD8^+$ T cell hyperfunction, characterized by an increase in the proportions of IFN-γ^+ and granzyme B^+CD8^+ T cells, in males after 4 weeks of HFMCDD feeding, which was sustained until end of treatment at 20 weeks[103].

In two independent HFMCDD studies (E01 and E03), flow cytometry analysis of bulk $CD4^+$ T cells (Fig 12A-C) and subsets were conducted in males and demonstrated minimal changes in $CD4^+$ T cell function between diet and chow study groups. In **E01**, no significant increases in the proportions of IFN-γ^+CD4^+ T cells were observed for the duration of the study (Fig 12D). However, a transient increase in the proportions of $GrzB^+CD4^+$ T cells were observed after 4 weeks of HFMCDD feeding (Fig 12E). After 16 weeks of diet feeding, there is trending increase in IL-17^+CD4^+ T cells in HFMCDD-fed males in comparison to controls (Fig 12F). Furthermore, there are increased proportions in T_{CM} and $T_{E/EM}$ $GrzB^+$ $CD4^+$ T cells at week 8 (Fig 12G). In **E03**, a transient increase in IFN-γ^+CD4^+ T cells was observed after 8 weeks of HFMCDD feeding (Fig 13A). No differences were observed in $GrzB^+$ or IL-17^+CD4^+ T cells at any timepoints in this group (Fig 13B-C). Nor were any differences observed in the proportions of T_{CM} or $T_{E/EM}$ $GrzB^+$ $CD4^+$ T cells at week 8 (Figure 13D). We were, therefore, unable to replicate the same results in the two independent studies.

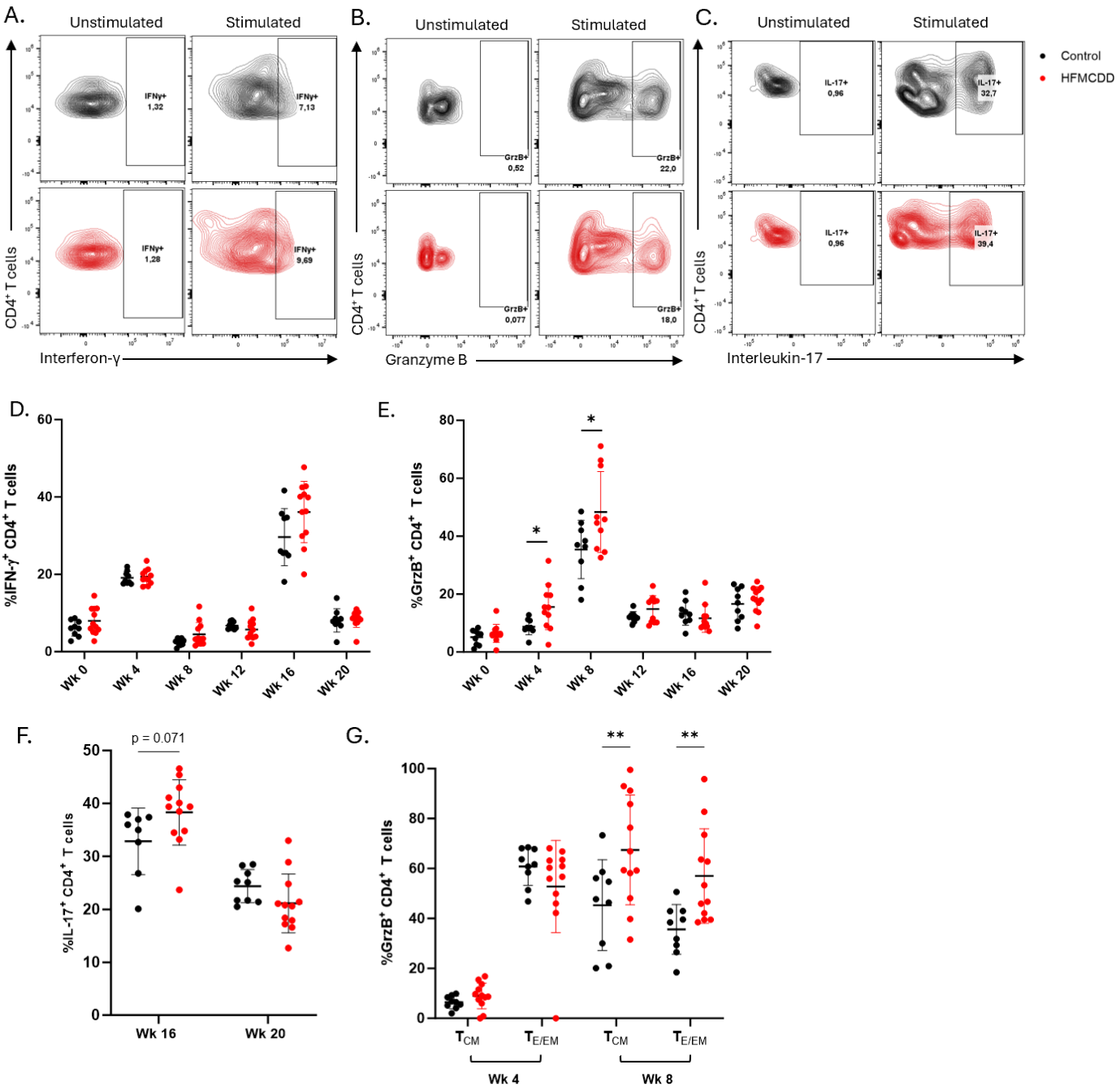
A.
Unstimulated
Stimulated
IFNγ+ 1,32
IFNγ+ 7,13
IFNγ+ 1,28
IFNγ+ 9,69
CD4+ T cells
Interferon-γ
B.
Unstimulated
Stimulated
GrzB+ 0,52
GrzB+ 22,0
GrzB+ 0,077
GrzB+ 18,0
CD4+ T cells
Granzyme B
C.
Unstimulated
Stimulated
IL-17+ 0,96
IL-17+ 32,7
IL-17+ 0,96
IL-17+ 39,4
CD4+ T cells
Interleukin-17
Control
HFMCDD
D.
%IFN-γ+ CD4+ T cells
Wk 0
Wk 4
Wk 8
Wk 12
Wk 16
Wk 20
E.
%GrzB+ CD4+ T cells
*
*
Wk 0
Wk 4
Wk 8
Wk 12
Wk 16
Wk 20
F.
p = 0.071
%IL-17+ CD4+ T cells
Wk 16
Wk 20
G.
**
**
%GrzB+ CD4+ T cells
TCM
TE/EM
TCM
TE/EM
Wk 4
Wk 8

Figure 12: Transient increase in the proportions of $GrzB^+CD4^+$ T cells in males after 4 weeks of HFMCDD feeding. Males were fed a HFMCDD *ad libitum f*or a duration of 20 weeks, while control mice were placed on a standard chow diet. At baseline and at intervals of 4 weeks, saphenous blood was collected and PBMCs were isolated. Representative responses of $CD4^+$ T cell function, demonstrating the expression **A)** IFN-γ, **B**) GrzB and **C)** IL-17. No difference in the proportions of **D**) IFN-γ^+CD4^+ T cells and transient increase in the proportions of **E)** $GrzB^+CD4^+$ T cells from 4-8 weeks of HFMCDD feeding. Trending increase in the proportions of **F)** IL-17^+CD4^+ T cells after 16 weeks of HFMCDD feeding. There is also an increase in the proportions of **G)** $GrzB^+$ T_{CM} and $T_{E/EM}$ $CD4^+$ T cells after 8 weeks of HFMCDD feeding. Data are presented as group means ±SD and statistically significant differences were determined using a one-tailed unpaired Student's t-test (*$p \leq 0.05$, **$p \leq 0.01$).

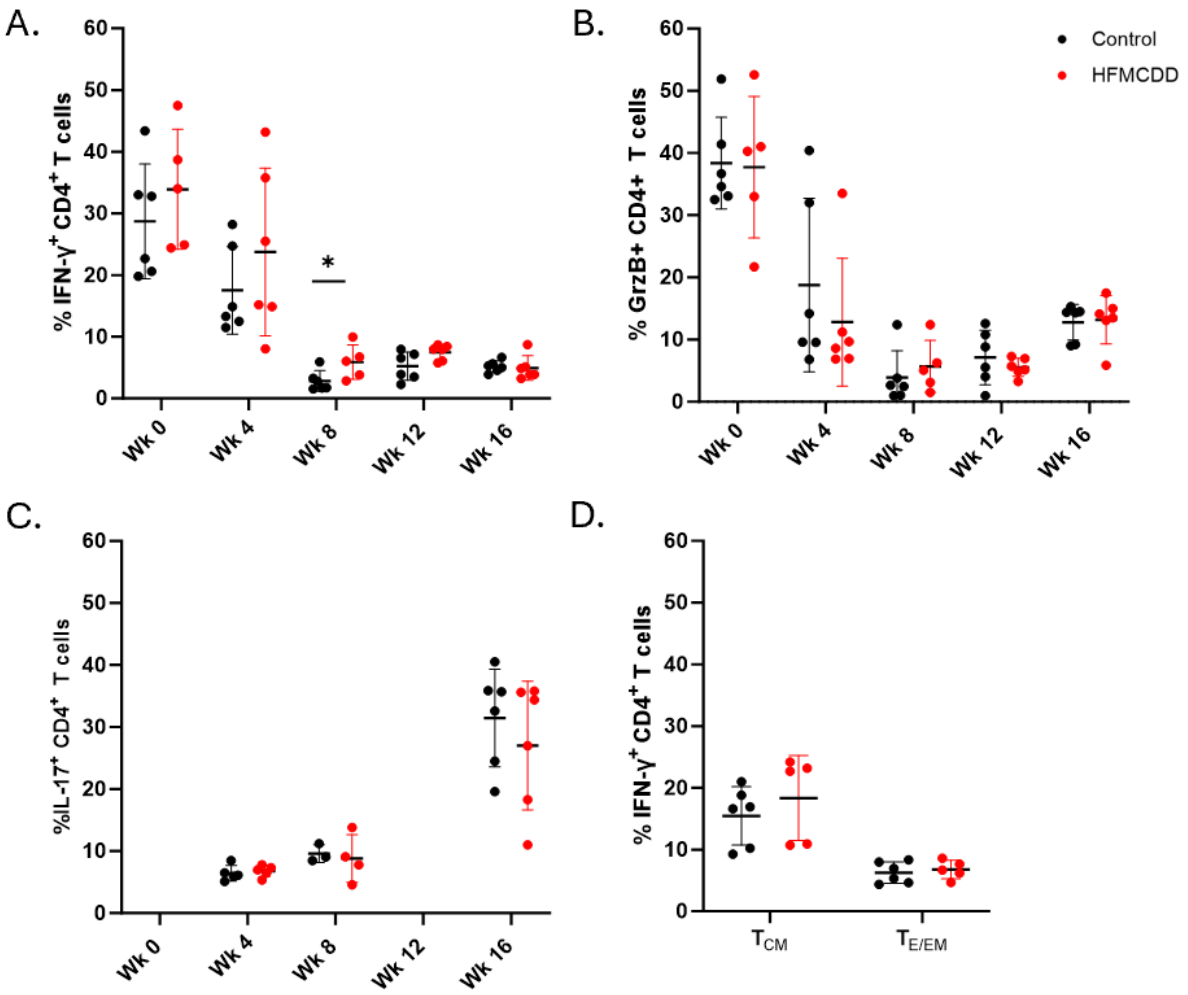

Figure 13: Transient increase in the proportions of IFN-γ$^+$CD4$^+$ T cells after 8 weeks of HFMCDD feeding. Males were fed a HFMCDD *ad libitum f*or a duration of 16 weeks, while control mice were placed on a standard chow diet. At baseline and at intervals of 4 weeks, saphenous blood was collected and PBMCs were isolated. There is a transient increase in the proportions of **A)** IFN-γ$^+$CD4$^+$ T cells after 8 weeks of diet feeding and no difference in proportions of **B)** GrzB$^+$ or **C)** IL-17$^+$CD4$^+$ T cells. No differences in proportions of **D)** IFN-γ$^+$ CD4$^+$ T cell subsets after 8 weeks of HFMCDD feeding. Data are presented as group means ±SD and statistically significant differences were determined using a one-tailed unpaired Student's t-test (*p≤0.05).

b. $CD4^+$ T cell function after 4-weeks of liver injury regression

After being fed an HFMCDD for 20 weeks, males from E01 were returned to the standard chow diet to study liver injury regression. At 20 weeks of treatment and at 2 and 4-weeks post-HFMCDD cessation, PBMCs were isolated from saphenous blood from the HFMCDD-fed and control mice and were stained with a variety of flow cytometry anti-mouse antibodies. Concurrent $CD8^+$ T cell studies in the Crawley Lab, demonstrated that $CD8^+$ T cell hyperfunction was sustained until peak treatment and was not observed during the regression period[103]. No differences were observed in IFN-γ^+, $GrzB^+$ or IL-17^+CD4^+ T cells between HFMCDD-fed males and controls at peak treatment or after (Fig 14A-C).

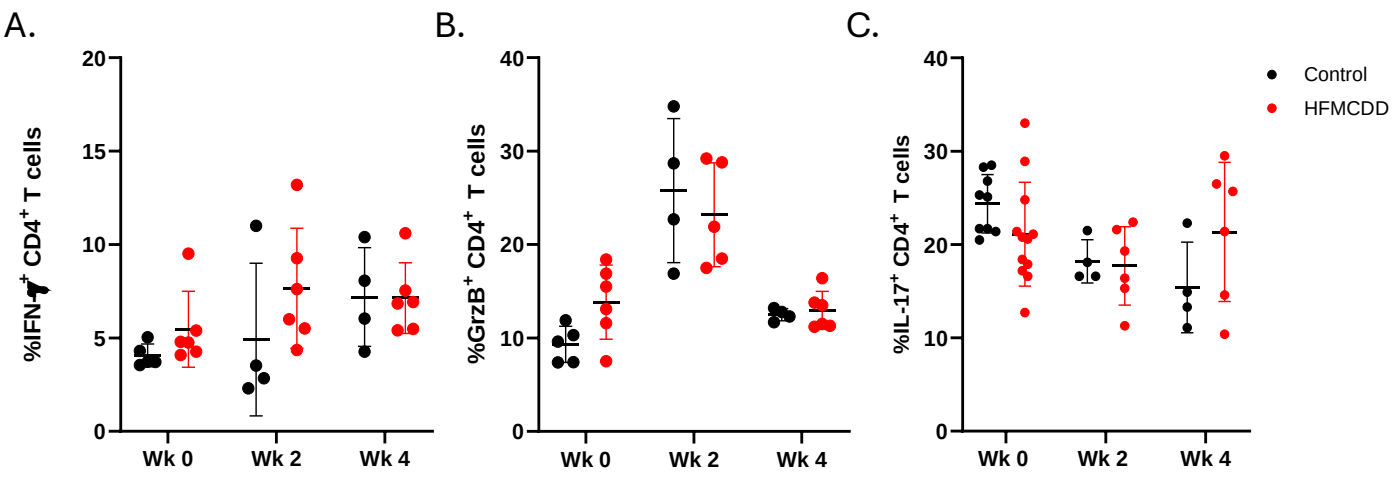

Figure 14: No changes to CD4$^+$ T cell function pre- and post-HFMCDD cessation. Males were fed a HFMCDD *ad libitum* for a duration of 20 weeks. After 20 weeks, the HFMCDD mice were returned to the standard chow diet for an additional 4 weeks. At baseline and at intervals of 4 weeks, saphenous blood was collected and PBMCs were isolated. No difference in proportions of **A)** IFN-γ^+, **B)** GrzB$^+$ or **C)** IL-17$^+$CD4$^+$ T cells after 4 weeks of HFMCDD cessation. Data are presented as group means ±SD and a one-tailed unpaired Student's t-test was performed, although no significant differences were found.

3.3.3. $CD4^+$ T cell function in HFMCDD-fed females

a. $CD4^+$ T cell function at peak HFMCDD treatment

At baseline and at intervals of 4 weeks, PBMCs were isolated from blood samples collected from HFMCDD-fed and control mice, then stained with a variety of flow cytometry antibodies. Concurrent $CD8^+$ T cell studies in the Crawley Lab, demonstrated $CD8^+$ T cell hyperfunction, characterized by an increase in the proportions of IFN-γ^+ and granzyme B^+CD8^+ T cells, in females after 8 weeks of HFMCDD feeding, which was sustained until 2 weeks post-HFMCDD cessation[103]. This finding demonstrates sex differences, as males developed $CD8^+$ T cell hyperfunction after only 4 weeks, as mentioned in Section 3.3.2a.

In two independent HFMCDD studies (E02 and E03), flow cytometry analysis of bulk $CD4^+$ T cells and subsets were conducted in females and demonstrated minimal changes in $CD4^+$ T cell function between diet and chow study groups. In **E02**, a transient increase in the proportions of IFN-γ^+CD4^+ T cells was observed in females after 8 weeks of HFMCDD feeding (Fig 15A). Furthermore, there was a persistent increase in the proportions of $GrzB^+CD4^+$ T cells after 8 weeks of HFMCDD feeding until end of treatment at 20 weeks (Fig 15B). Lastly, there was a trending increase in the proportions of IL-17^+CD4^+ T cells after 16 weeks of diet feeding (Fig 15C). These findings demonstrate sex differences, as males developed transient $CD4^+$ T cell hyperfunction, characterized by an increase in the proportions of $GrzB^+CD4^+$ T cells, after only 4 weeks, as well as a trending increase in IL-17^+CD4^+ T cells after 16 weeks (Refer to Section 3.3.2b). Furthermore, there was an increase in the proportions in T_{CM} $GrzB^+$ $CD4^+$ T cells at week 20 of HFMCDD feeding (Fig 15E), while no differences were observed in T_N or $T_{E/EM}$ subsets. In **E03**, there were transient increases in the proportions of IFN-γ^+ and $GrzB^+CD4^+$ T cells after 12 weeks of HFMCDD feeding, in comparison to controls, which was not maintained thereafter (Fig 16A-B).

No significant differences were observed in the proportions of IL-17^{+}CD4^{+} T cells at any timepoints (Fig 16C). In this group, there are increases in the proportions of GrzB^{+} T_{CM} and $T_{E/EM}$ CD4^{+} T cells after 12 weeks of HFMCDD feeding, in comparison to controls.

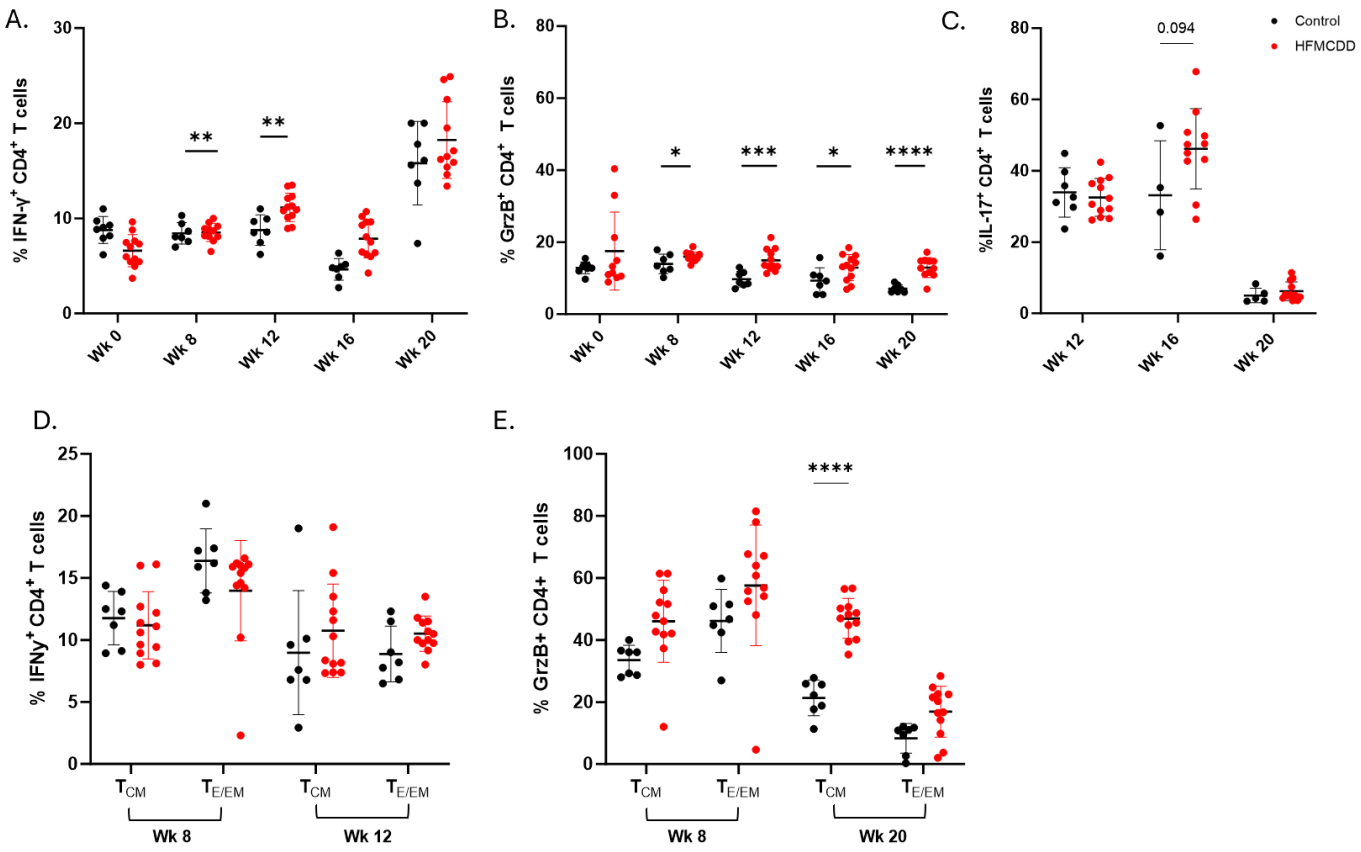

Figure 15: Persistent CD4$^+$ T cell hyperfunction in females. C57BL/6 females were fed a HFMCDD *ad libitum f*or a duration of 20 weeks, while control mice were placed on a regular chow diet. At baseline and at intervals of 4 weeks, saphenous blood was collected and PBMCs were isolated. There is a transient increase in the proportions of **A)** IFN-γ^+CD4$^+$ T cells after 12 weeks of diet feeding, and a persistent increase in the proportions of **B)** GrzB$^+$CD4$^+$ T cells from 8 weeks of HFMCDD feeding until end of treatment. Trending increase in proportions of **C)** IL-17$^+$CD4$^+$ T cells after 16 weeks of HFMCDD feeding. No differences observed in the proportions of **D)** IFN-γ^+ T_{CM} and $T_{E/EM}$ CD4$^+$ T cells at weeks 8 and 12 of HFMCDD feeding. Proportions of **E)** GrzB$^+$ T_{CM} and $T_{E/EM}$ CD4$^+$ T cells were increased after 20 weeks of diet. Data are presented as group means ±SD and statistically significant differences were determined using a one-tailed unpaired Student's t-test (*p≤0.05,**p≤0.01,*** p≤0.001,****p≤0.0001).

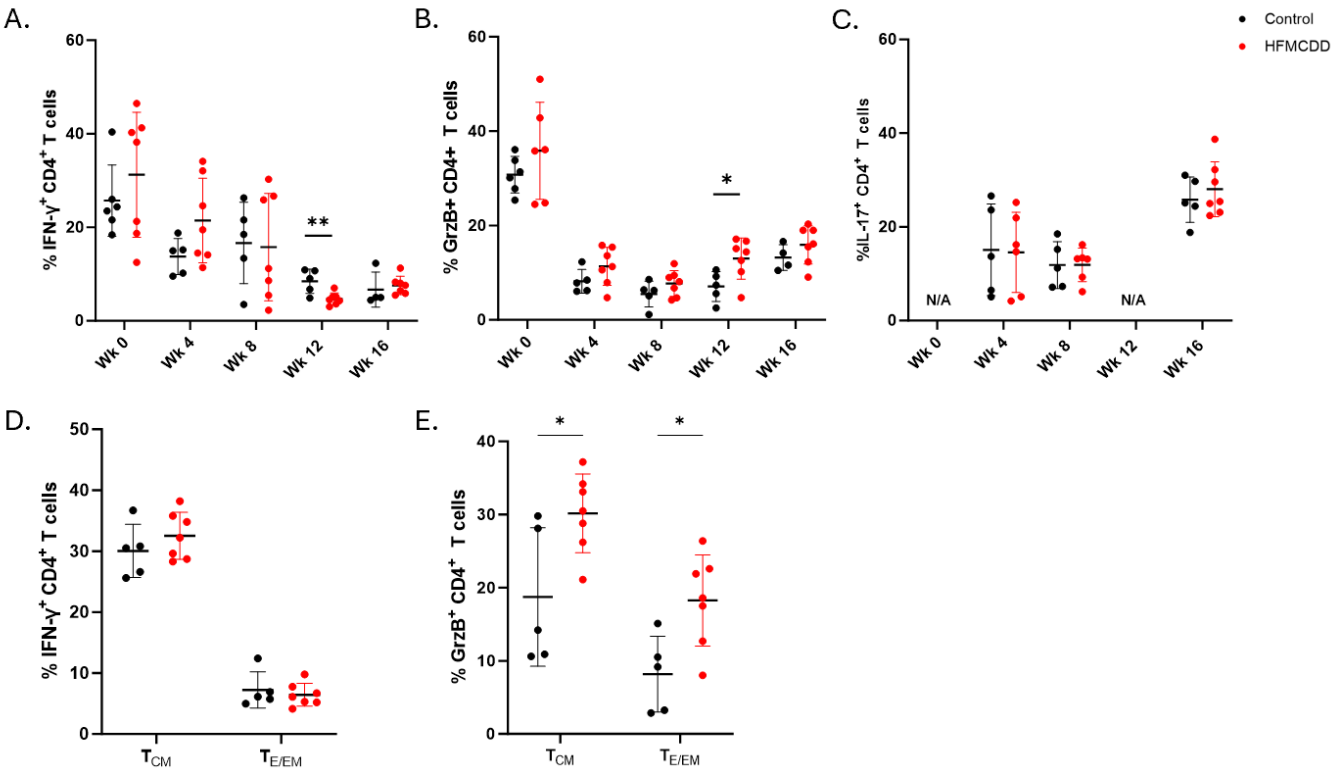

Figure 16: Transient increase in IFN-γ$^+$ and GrzB$^+$CD4$^+$ T cells after 12 weeks of HFMCDD feeding in females. C57BL/6 females were fed a HFMCDD *ad libitum f*or a duration of 16 weeks, while control mice were placed on a regular chow diet. At baseline and at intervals of 4 weeks, saphenous blood was collected and PBMCs were isolated. There are transient increases in the proportions of **A)** IFN-γ$^+$ and **B)** GrzB$^+$CD4$^+$ T cells after 12 weeks of diet feeding**.** No difference in the proportions of **C)** IL-17$^+$CD4$^+$ T cells. No differences observed in the proportions of **D)** IFN-γ$^+$ CD4$^+$ T cell subsets but increases in the proportions of **E)** GrzB$^+$ T_{CM} and $T_{E/EM}$ CD4$^+$ T cells were seen after 12 weeks of HFMCDD feeding. Data are presented as group means ±SD and statistically significant differences were determined using a one-tailed unpaired Student's t-test (*p≤0.05, **p≤0.01).

b. $CD4^+$ T cell function after 4-weeks of liver injury regression

After being fed an HFMCDD for 20 weeks, females returned to the standard chow diet to study liver injury regression. At 20 weeks of diet feeding, 2 weeks and 4 weeks post-HFMCDD cessation, PBMCs were isolated from saphenous blood collections, and stained with a variety of flow cytometry antibodies (refer to section 2.9). Concurrent $CD8^+$ T cell studies in the Crawley Lab, demonstrated that $CD8^+$ T cell hyperfunction was sustained after 8 weeks of HFMCDD feeding and remained until 2 weeks post-HFMCDD cessation[103]. Similarly, there was an increase in the proportions of $GrzB^+CD4^+$ T cells in HFMCDD-fed mice after 8 weeks until 2 weeks post-HFMCDD cessation. No differences were observed in the proportions of IFN-γ^+ or IL-17^+CD4^+ T cells (Fig 17A-C). This finding demonstrates clear sex differences, as the $CD8^+$ T cell hyperfunction observed in males was not sustained post-HFMCDD cessation (mentioned in Section 3.3.2b) as seen here in females.

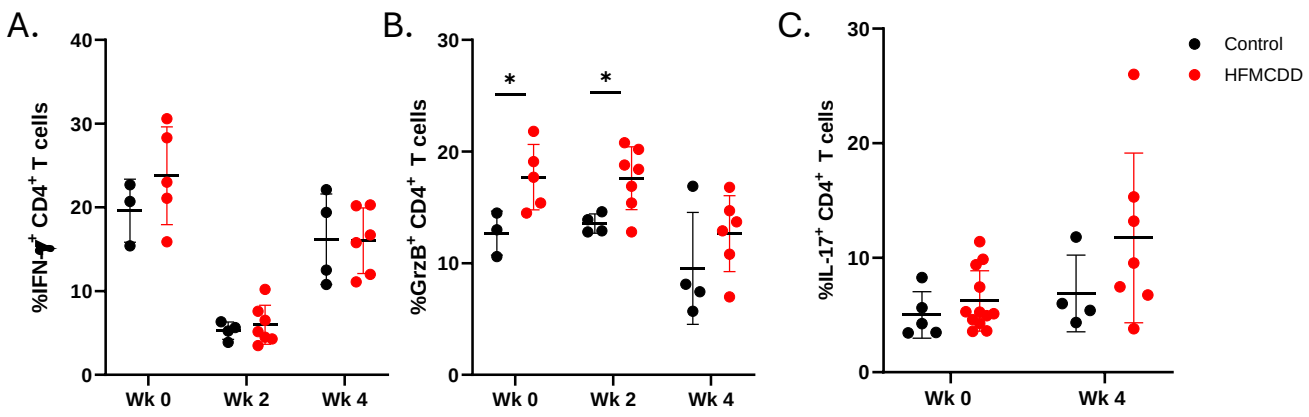

Figure 17: CD4$^+$ T cell hyperfunction resolved after 2 weeks of HFMCDD cessation. Females were fed a HFMCDD *ad libitum* for 20 weeks, while control mice were placed on a standard chow diet. After 20 weeks, the HFMCDD mice were returned to the standard chow diet for 4 weeks. At baseline and at intervals of 4 weeks, saphenous blood was collected and PBMCs were isolated. No difference in the proportions of **A)** IFN-γ^+CD4$^+$ T cells. An increase in the proportions of **B)** GrzB$^+$CD4$^+$ T cells was observed at 20 weeks of diet feeding and 2 weeks post-HFMCDD cessation. No differences in the proportions of **C)** IL-17$^+$CD4$^+$ T cells observed during regression. Data are presented as group means ±SD and statistically significant differences were determined using a one-tailed unpaired Student's t-test (*p≤0.05).

3.3.4. $CD4^+$ and $CD8^+$ T cell infiltration in HFMCDD-fed mice

For a duration of 16-21 weeks, five groups of C57BL/6 were fed a high-fat methionine and choline deficient diet (HFMCDD) *ad libitum*. At endpoint (week 16-21) and 4 weeks after returning to the standard chow diet, mouse livers were collected from HFMCDD-fed mice and controls. Animals were euthanized and liver sections were sent to the Louise Pelletier Histology Core Facility (University of Ottawa) for paraffin embedding, sectioning, and staining. A selection of FFPE liver blocks from the control, HFMCDD and HFMCDD-cessation groups were sent to the histology core for triple immunofluorescence (IF) staining (Fig 18A-C).

Experimental mice from **E01**, **E02** and **E03** were combined together for these analyses, as the focus was to observe overall T cell infiltration differences, sex differences and the relationship between T cell infiltration and liver injury severity. After 20 weeks of diet feeding, HFMCDD-fed mice demonstrated increases in the proportions of intrahepatic $CD4^+$ and $CD8^+$ T cells in comparison to controls. Interestingly, these changes were resolved after 4 weeks of diet cessation. Furthermore, it was observed that $CD4^+$ T cells from controls expressed greater IFN-γ^+ than HFMCDD-fed or post-HFMCDD cessation mice (Fig 18D-G). When analyzing samples for double positives, no significant increases in the proportions of $CD4^+GrzB^+$, $CD4^+$IFN-γ^+, $CD8^+GrzB^+$, $CD8^+$IFN-γ^+ or $GrzB^+$IFN-γ^+ T cells were observed (Fig 18H-I).

When studying sex differences, we observed greater proportions of infiltrated $CD4^+$ and $CD8^+$ T cells in HFMCDD-fed males in comparison to HFMCDD-fed females. Males also demonstrated partial resolution 4 weeks post-HFMCDD cessation (Fig 19A-B). Lastly, positive correlations were shown between $CD4^+$ and $CD8^+$ T cell count per area and liver injury scores (ie. fibrosis, steatosis), although $CD4^+$ T cell infiltration proved stronger correlations with liver fibrosis and steatosis scores ($r = 0.734$ and 0.580, respectively) than $CD8^+$ T cell infiltration ($r = 0.528$ and 0.350, respectively) (Fig 20A-D).

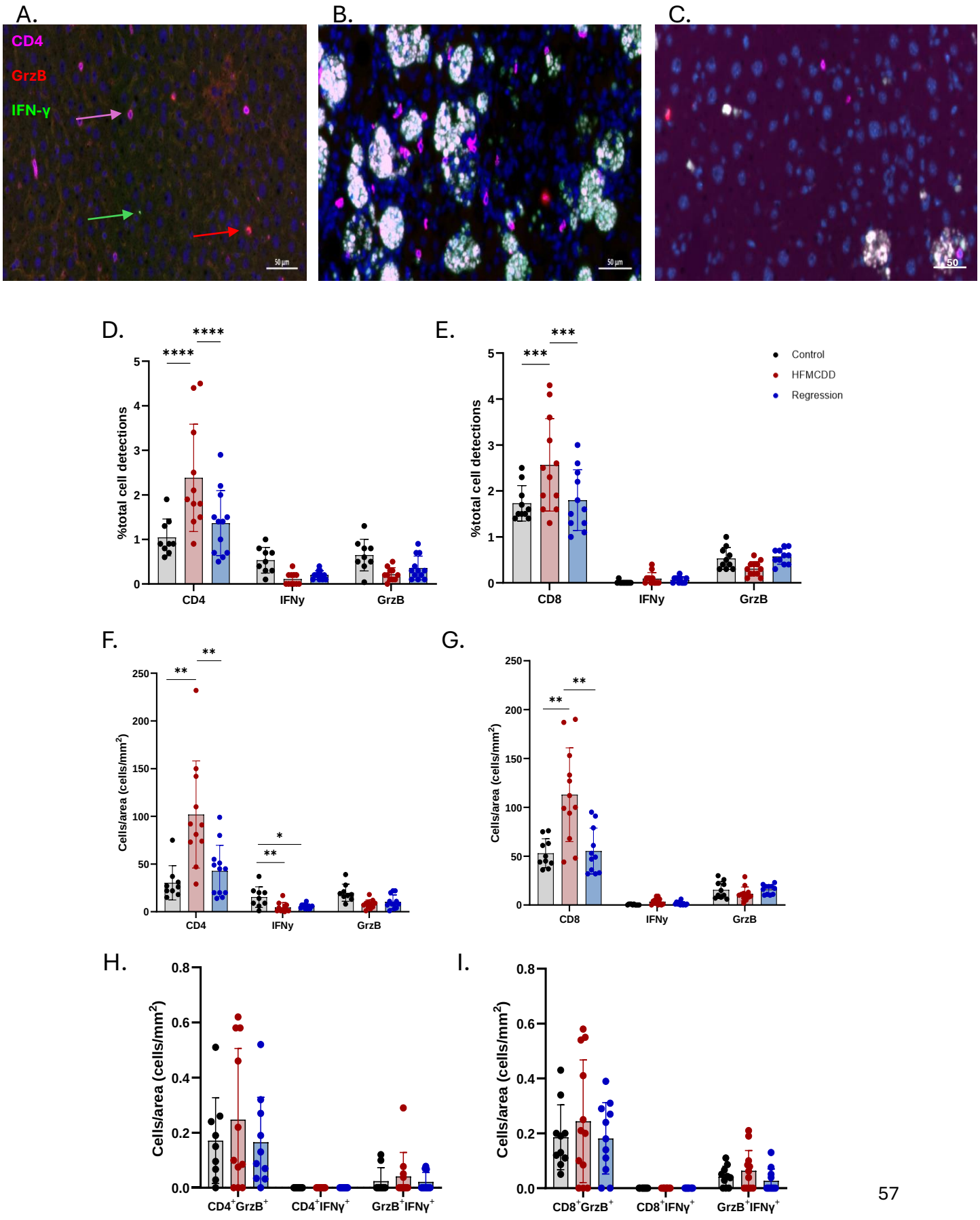
A.
CD4
GrzB
IFN-γ
B.
C.
D.
%total cell detections
CD4
IFNy
GrzB
E.
Control
HFMCDD
Regression
CD8
F.
Cells/area (cells/mm²)
G.
H.
CD4⁺GrzB⁺
CD4⁺IFNγ⁺
GrzB⁺IFNγ⁺
I.
CD8⁺GrzB⁺
CD8⁺IFNγ⁺
GrzB⁺IFNγ⁺

Figure 18: Increased $CD4^+$ and $CD8^+$ T cell infiltration in HFMCDD-fed mice, which resolve after 4 weeks of diet cessation. Mice were fed a HFMCDD *ad libitum* for 20 weeks, after which, were returned to the standard chow diet for an additional four weeks. After 20 weeks and 4 weeks post-HFMCDD cessation, livers were collected and prepped for triple IF staining. Representative liver triple IF-stained histology images for **A)** control, **B)** HFMCDD-fed mouse and **C)** HFMCDD-mouse 4 weeks post-HFMCDD cessation. Percentage of total cell detections for **D)** CD4, IFN-γ and GrzB and **E)** CD8, IFN-γ and GrzB. Cells/area for **F)** CD4, IFN-γ and GrzB and **G)** CD8, IFN-γ and GrzB. Cells/area for **H)** $CD4^+$ T cells and **I)** $CD8^+$ T cells expressing double positives. Data are presented as group means ±SD. Statistical analysis was carried out by two-way analysis of variance (ANOVA) followed by Tukey-Kramer test for multiple comparisons (*$p \leq 0.05$,**$p \leq 0.01$,*** $p \leq 0.001$,****$p \leq 0.0001$). Scale bar = 50 μM.

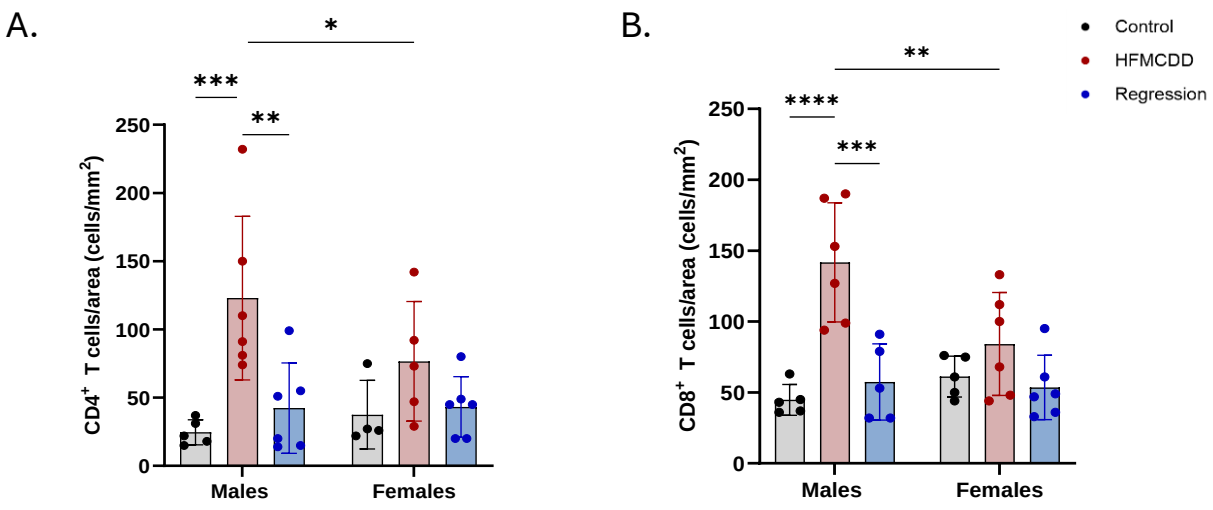

Figure 19: Increased CD4$^+$ and CD8$^+$ T cell infiltration in males. Mice were fed a HFMCDD *ad libitum* for 20 weeks, after which, were returned to the standard chow diet for an additional four weeks. After 20 weeks and 4 weeks post-HFMCDD cessation, livers were collected and prepped for triple IF staining. Increased **A)** CD4$^+$ and **B)** CD8$^+$ T cell infiltration in HFMCDD-fed males compared to females, and resolution in the regression study group. Data are presented as group means ±SD and statistical analysis was carried out by two-way analysis of variance (ANOVA) followed by Tukey-Kramer test for multiple comparisons (*p≤0.05).

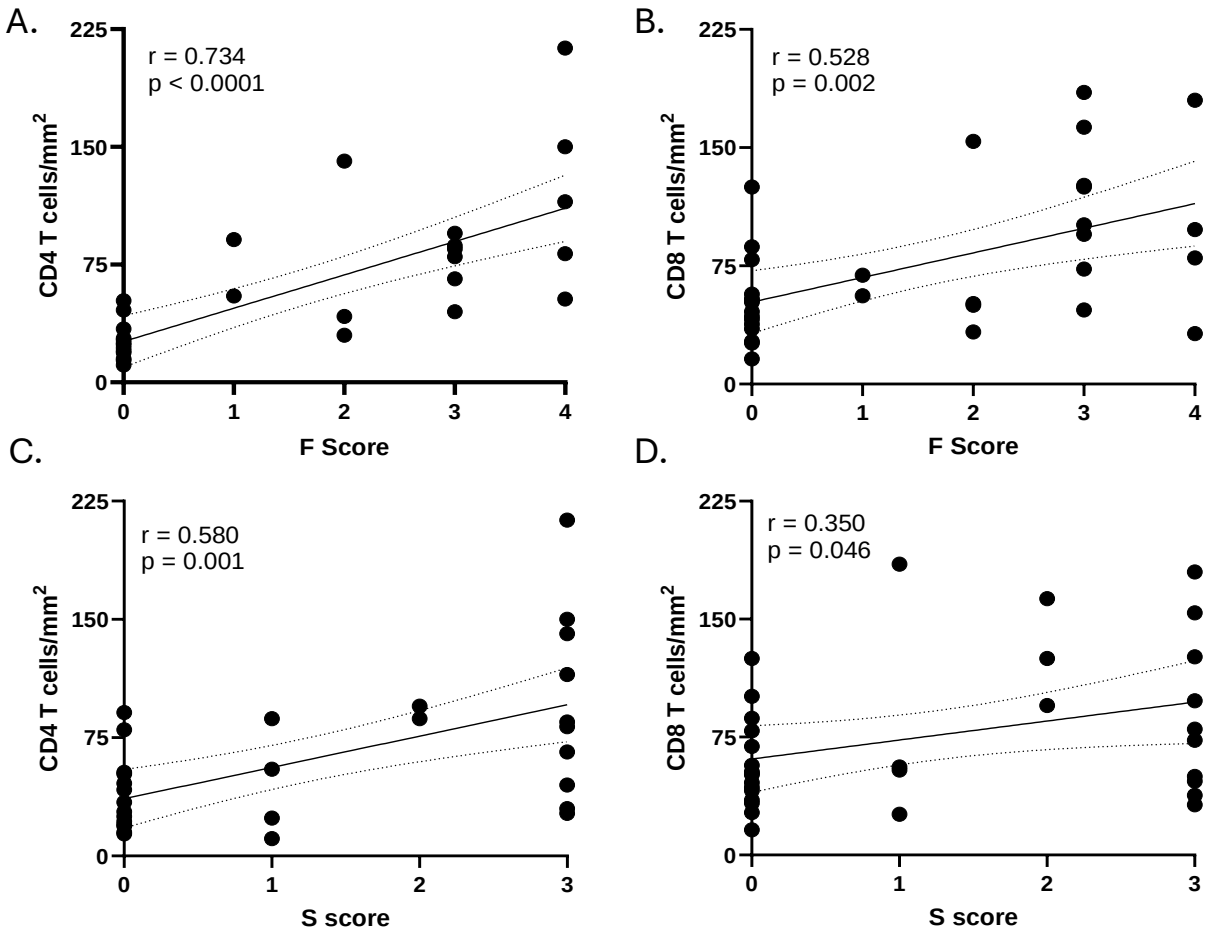

Figure 20: CD4$^+$ and CD8$^+$ T cell infiltration correlates with liver fibrosis and steatosis. Mice were fed a HFMCDD *ad libitum* for 20 weeks, after which, were returned to the standard chow diet for an additional four weeks. After 20 weeks and 4 weeks post-HFMCDD cessation, livers were collected and prepped for triple IF staining. The relationships between liver fibrosis severity and **A)** CD4$^+$ T cells and **B)** CD8$^+$ T cells, and between liver steatosis severity and **C)** CD4$^+$ T cells and **D)** CD8$^+$ T cells are shown. Data are presented as group means ±SD. Statistical analysis was carried out by correlation analysis followed by non-linear regression.

CHAPTER 4: DISCUSSION

In this thesis, both human and mouse models of liver disease were used to study the impact of MASLD/MASH on circulating and intrahepatic $CD4^+$ T cells, specifically function and infiltration, with the addition of its implications on $CD8^+$ T cells. MASLD/MASH patients with advanced liver fibrosis demonstrated $CD4^+$ T cell hyperfunction, with elevated IFN-γ and TGF-β expression, compared to those with minimal fibrosis and healthy controls. The HFMCDD mouse model reliably mimics MASH-related liver pathology, inducing advanced steatosis and fibrosis, with moderate ballooning and inflammation. Advanced liver injury was accompanied by bulk, T_{CM} and $T_{E/EM}$ $CD4^+$ T cell hyperfunction, characterized by increased proportions of IFN-γ^+ and $GrzB^+CD4^+$ T cells. While $CD4^+$ and $CD8^+$ hyperfunction was transient in nature in HFMCDD-fed males, in females, it was persistent until 2 weeks after returning to a regular chow diet. These findings suggest that $CD4^+$ T cell hyperfunction is associated with advanced liver injury, both fibrosis alone as well as fibrosis with steatosis, in chronic liver disease.

4.1 $CD4^+$ T cell function in MASLD/MASH patients

MASLD is now the most common chronic liver disease worldwide (32%), predominantly affecting men (40%) compared to women (26%)[45]. Individuals with T2DM, are twice more likely to develop MASLD, with a prevalence of 65% within this group[78,138]. The lipotoxicity associated with MASLD causes metabolic dysfunction, insulin resistance, prompting the secretion of adipokines and proinflammatory cytokines, and cellular damage, triggering immune cell infiltration into the liver and fibrogenesis[50]. It was also found that many immune cell abnormalities occur throughout the progression of MASLD to MASH, such as increased expression of IFN-γ^+ and TGF-β^+CD4^+ T cell subset[112,139,140]. In this thesis, we observed elevated expression of IFN-γ

and TGF-β in bulk circulating $CD4^+$ T cells in MASLD/MASH individuals with advanced liver fibrosis in comparison to those with minimal fibrosis or healthy individuals (Fig 2F-G).

In MASLD pathogenesis, an important contributing factor is body fat distribution, which greatly differs between both sexes. Females accumulate subcutaneous adiposity, while males accumulate visceral adiposity, promoting localized inflammation and accelerating liver fibrosis progression[136,137]. Males also tend to exhibit more severe steatosis/steatohepatitis, more advanced fibrosis, elevated pro-inflammatory cytokine levels, higher liver tumour incidence and increased overall mortality, making them more susceptible to developing MASH, cirrhosis and HCC[8,80]. These sex differences are related to hormonal changes associated with age, as men typically develop MASLD during adulthood, with a decline after middle age (50–60 years old) and women develop MASLD after menopause (~50 years old)[81]. This phenomenon occurs due to the reduction of estrogen levels in women following menopause, thus losing the protective effect of estrogen against the progression of MASLD. Estrogen typically inhibits the proliferation of HSC, thus preventing the development of fibrotic tissue in the liver[141]. In this study group, the mean age of MASH-diagnosed men with minimal and advanced liver fibrosis were 47.6 and 67.0 years old, respectively. While in MASH-diagnosed women, the mean age was 46.4 and 61.7 years old, respectively (Table 2), which parallels with the hormonal changes observed in menopause. However, small sample sizes here restricted the capacity to conclude sex effects in T cell functions.

4.2 CCl_4-induced liver fibrosis murine model

Since HCV cannot infect wild-type rodents, the hepatotoxin model using CCl_4 was developed to replicate HCV-induced liver fibrosis, in the absence of viral infection[118,119]. Long-term exposure to CCl_4 is known to cause hepatotoxicity with resulting fibrosis, cirrhosis and eventual HCC, and progressive loss of hepatic function. The causes of CCl_4-induced liver injury

include toxic effects caused by reactive metabolites, ROS, inflammatory responses and imbalances between cellular damage and repair, which all contribute to inflammation, oxidative stress and fibrosis. The ensuing oxidative stress will additionally initiate the production of inflammatory cytokines, hepatocyte death, inflammation, and further promotes hepatic fibrogenesis[142]. The accumulation of fibrotic tissue over time is increasingly associated with immune dysfunction, specifically the Th17/Treg ratio which increases as fibrosis advances, and contributes to their poor clinical outcomes[20,143]. The Crawley lab has been able to induce advanced liver fibrosis (F3-F4) in C57BL/6 mice after 12-16 weeks of hepatotoxin administration in 10 consecutive cohorts[100,101].

In this thesis, the first cohort of C57BL/6 mice were injected twice weekly (i.p.) with CCl_4 for a duration of 21 weeks. During this treatment, advanced liver fibrosis was induced (Fig 5D), predominantly developing F3 fibrosis in males (Fig 5E), and highly variable scores (F0-4) in females (Fig 5F). In a secondary cohort, mice followed the same treatment for a duration of 16 weeks and produced similar results (Fig 5G-I). These findings seem consistent with those found in rats exposed to CCl_4 injections, where it was found that the severity of liver fibrosis in females was less significant than that of males. It is believed that the antifibrogenic effect of estrogen plays a protective role against CCl_4 by suppressing the synthesis and release of cytokines (e.g. TGF-β) and growth factors (e.g. PDGF), thus altering HSC activation and proliferation.[144] Similarly, in HCV-infected individuals, it was found that men tend to develop more severe liver fibrosis than women, although these sex differences did not persist after DAA therapy[145].

4.3 $CD4^+$ T cell function in CCl_4-induced liver fibrosis murine model

During chronic HCV infection, both HCV-specific $CD4^+$ and $CD8^+$ T cells become functionally exhausted[146]. This T cell exhaustion is in part caused by the loss of HCV-specific $CD4^+$ T cells, which are subsequently required for the induction of effector $CD8^+$ T cell functions[147,148]. As central mediators of adaptive immunity, $CD4^+$ T cells facilitate both $CD8^+$ T cell responses and antibody responses to viral pathogens[34]. By producing cytokines, such as IFN-γ and IL-2, $CD4^+$ T cells direct the differentiation of $CD8^+$ T cells, which are key players in viral control and release immunoregulatory cytokines[93,149]. In the Crawley lab, the CCl_4-induced liver fibrosis murine model demonstrated an association with generalized $CD8^+$ T cell hyperfunction, characterized by increases in the proportions of IFN-γ^+ and $GrzB^+CD8^+$ T cells in treated mice compared to controls[100]. Preliminary data also suggested that a significant increase in the proportions of $GrzB^+CD4^+$ T cells was found in CCl_4-treated mice *(Crawley, unpublished*). Interestingly, studies by Sun et al., showed that this CCl_4 model impairs $CD4^+$ T cells, and triggers an imbalance in the ratio of intrahepatic Tregs/Th17 cells, contributing to the progression of fibrosis via HSC activation[150]. In this thesis, we observed a transient increase in the proportions of bulk circulating $GrzB^+$ and TNF-α^+CD4^+ T cells at the 18 week-timepoint of CCl_4 treatment of one of our cohorts (Fig 6F-G). Unlike the first 5 cohorts previously studied in the CCl_4 model, $CD8^+$ T cell hyperfunction was not replicated here, and this may reflect in these data, that show $CD4^+$ T cell hyperfunction was either transient or absent.

4.4 HFMCDD-induced liver injury murine model

The HFMCDD model closely mimics the histopathological features of human MASH, with ballooning hepatocyte degeneration in addition to fat accumulation, inflammation and fibrosis[123,124]. The combination of a high-fat diet and methionine and choline deficiencies,

respectively promotes weight gain and liver damage, and impairs metabolic pathways, thus promoting weight loss and liver fibrosis, reflective of the progression to MASH[125]. Moderate inflammation and ballooning as well as advanced steatohepatitis (S3) are expected after 3 weeks of this diet feeding, and moderate (F1-2) and advanced liver fibrosis (F3) after 6-9 and 12 weeks, respectively[126]. Relative to other high-fat diet models, the HFMCDD induces chronic liver disease pathologies relatively quickly and induces advanced fibrosis within 12-16 weeks. This is also a comparable time frame to that of CCl_4 model, which requires a minimum of 12 weeks to start seeing altered immune functions and advanced liver injuries[100]. The added value of the HFMCDD model is that it highlights that severe steatosis, achieved within 4 weeks while absent in CCl_4, resulted in either transient or lasting T cell hyperfunction. Therefore, steatosis, in addition to advanced fibrosis, also has a role in inducing T cell hyperfunction.

Combining the findings of two male cohorts, we observed progression of liver damage, as measured by steatosis and fibrosis, with moderate-to-advanced fibrosis (mean F3±SD) and steatosis (mean S2-3±SD) at 16 weeks of diet feeding (Fig 10B), and advanced fibrosis (mean F4±SD) and advanced liver steatosis (mean S3±SD) at 21 weeks of diet feeding (Fig 8F). Then, a similar pattern of liver damage was observed in females at 16 weeks, with moderate-to-advanced liver fibrosis (mean F2-3±SD) and advanced liver steatosis (S3±SD) (Fig 10B). However, females did not progress as much as males, with moderate-to-advanced liver fibrosis (mean F2-3±SD) and advanced liver steatosis (S3±SD) developed at 21 weeks of diet feeding (Fig 9E). Multiple studies have pointed out sex differences in the pathophysiology of MASLD, which seem to be reflected in this mouse model. For example, in humans, males are more likely to developing MASH, fibrosis and cirrhosis, and are diagnosed with HCC two to four times more often than females[80]. These differences are thought to be caused by the hormonal fluctuations associated with menopause, after

which, females lose the protection against liver damage provided by estrogens[83,84,136]. By the end of the experiment, the female mice were approximately 31 weeks old and approaching the equivalent age of menopause in mice, which begins around 9 months (36 weeks) of age[151].

After a period of 21 weeks on an HFMCDD, the first cohort of males and females were returned to a regular chow diet to evaluate potential liver injury regression and associated T cell phenotyping over 4 weeks. The mean fibrosis score of males reduced from F4 to F3, a clinically relevant decrease given its association with HCC risk in humans, and steatosis reduced to control levels (S0-2). In females, fibrosis scores remained unchanged, while steatosis completely resolved (Fig 11A-B). Clinically, it is possible to reverse the fat accumulation in the liver by managing metabolic factors, such as weight, cholesterol, blood pressure and blood sugar, but once MASH progresses to advanced fibrosis (F3-F4) and cirrhosis, the damage is permanent[152]. Estrogen deficiency, as observed in menopause, also slows down wound healing and tissue remodelling processes, thus potentially preventing liver fibrosis regression in this model[153]. These experiments clearly indicate the potential for tissue repair and remodelling against advanced steatosis in MASLD, with a predominance for females.

4.5 $CD4^+$ T cell function in HFMCDD-induced liver injury murine model

In MASLD and MASH, $CD4^+$ and $CD8^+$ T cells have been shown to promote MASLD progression by inducing inflammation, hepatocyte death and fibrosis, through the secretion of IFN-γ, perforin and granzymes[76,102]. A humanized mouse model for diet-induced MASLD showed that subsets of $CD4^+$ T cells, specifically IL-17-secreting Th17 and IFN-γ-secreting Th1, play a key role in the progression of steatosis to fibrosis and correlate positively with disease progress in MASH-HCC[71,72]. Recent HFMCDD studies in the Crawley Lab demonstrated $CD8^+$ T cell hyperfunction in diet-fed males, characterized by an increase in the proportions of IFN-γ^+ and

$GrzB^+CD8^+$ T cells, after only 4 weeks, which was sustained until end of treatment at 20 weeks. Similarly, in females, there was $CD8^+$ T cell hyperfunction after 8 weeks of HFMCDD feeding, sustained until 2 weeks post-HFMCDD cessation[103].

In the first cohort of males, after 4 weeks of HFMCDD feeding, there was a transient increase in the proportions of $GrzB^+CD4^+$ T cells and a trending increase in $IL\text{-}17^+CD4^+$ T cells (Fig 12E-F). This correlates with a timepoint at which advanced steatosis is expected to have developed, in the absence of fibrosis[126]. Similarly to $CD8^+$ T cells, no $CD4^+$ T cell hyperfunction was maintained in males during the regression period. In the first cohort of females, there was a transient increase in the proportions of $IFN\text{-}\gamma^+CD4^+$ T cells after 8 weeks of HFMCDD feeding (Fig 15A), and a persistent increase in the proportions of $GrzB^+CD4^+$ T cells (Fig 15B). This $CD4^+$ T cell hyperfunction was maintained until 2 weeks post-HFMCDD cessation (Fig 17B), identically to $CD8^+$ T cells, at a timepoint where we have observed complete steatosis reversal, while fibrosis remained unchanged. In addition to these sex differences in bulk $CD4^+$ T cell hyperfunction, there were increased proportions in T_{CM} and $T_{E/EM}$ $GrzB^+$ $CD4^+$ T cells at week 8 in males (Fig 12G), which was not observed in females. Due to experimental errors, we were unable to perform $CD4^+$ T cell functional analyses at week 4, the timepoint at which we observed $CD4^+$ T cell hyperfunction in males. Sex differences could therefore not be performed and an additional cohort of HFMCDD females was studied. In this second cohort, we observed transient increases in the proportions of $IFN\text{-}\gamma^+$ and $GrzB^+CD4^+$ T cells only after 12 weeks of HFMCDD feeding (Fig 16A-B), and, we were, therefore, unable to replicate the earlier findings. Conclusive sex differences in this study regarding T cell hyperfunction could not be established due to the variability in the results between cohorts, and further experiments would need to be conducted. Interestingly, this model adds an association between T cell hyperfunction and liver steatosis, complementing the one made to liver

fibrosis in previous cohorts of the CCl_4 model. These findings appear to parallel established research, stating that $CD4^+$ T cell dysfunction is associated with the progression of steatosis-to-fibrosis in MASLD/MASH. Furthermore, this highlights steatosis as a potential therapeutic target to overcome immune dysfunction in those affected by MASLD and its complications.

4.6 T cell infiltration in HFMCDD-induced liver injury murine model

MASLD is the leading cause of CLD worldwide, with a prevalence of 32% in the adult population, predominantly affecting men[45]. About 20-30% of those diagnosed with MASLD will develop the progressive inflammatory form of the disease, MASH, characterized by steatosis, ballooning, and inflammation. One of the key histopathological features of MASH is elevated immune cell infiltration, such as T cells, NK cells and macrophages, but how these contribute to MASLD pathophysiology remains to be understood[77,112,154]. Both murine and human studies, demonstrated significant increases in intrahepatic $CD4^+$ and $CD8^+$ T cells, as well as macrophages ($CD68^+$), which localized to fibrotic regions, suggesting a role for $CD4^+$ T cells in diet-induced liver inflammation and steatosis-to-fibrosis progression[72]. It was also found that intrahepatic infiltration of $CD8^+$ T cells and macrophages is driven by $CD4^+$ T cells, while the depletion of $CD4^+$ T cells reduced immune infiltration, inflammation and fibrosis[113].

In this thesis, C57BL/6 mice were fed a HFMCDD for a duration of 21 weeks, then returned to a standard chow diet for an additional 4 weeks for liver regression studies. After the initial 21 weeks, there were increases in intrahepatic $CD4^+$ and $CD8^+$ T cells in comparison to controls, confirming previous reports listed above. These changes seemed to have resolved themselves following 4 weeks of liver injury regression (Fig 18D-G). There were also increased proportions of infiltrated $CD4^+$ and $CD8^+$ T cells in males compared to females, which resolved after regression as well (Fig 19A-B). In order to prevent autofluorescence from interfering with triple IF staining,

proper tissue perfusion needs to be performed since red blood cells naturally fluoresce across multiple wavelengths, rendering it difficult to distinguish assay fluorescence from endogenous fluorescence[155]. Unfortunately, the liver sections collected from the CCl_4 study groups were not perfused and could not be stained for these experiments. Although, there is little research discussing sex differences in intrahepatic T cell infiltration, studies have demonstrated fewer immune cells, specifically NK cells, in the liver of female mice with MASLD than males[156]. Most importantly, positive correlations were observed between liver injury scores (fibrosis and steatosis) and $CD4^+$ and $CD8^+$ T cell infiltration (Fig 20 A-D). This parallels studies that found a positive correlation between T cell infiltration and the deterioration of liver function, where the number of T cells (and macrophage infiltrates) was significantly higher in patients with hepatic dysfunction[157]. The immunohistochemistry findings from this thesis highlight T cell infiltration in the progression and regression of liver injury, namely steatosis, in MASH. In addition to the aforementioned, this further highlights steatosis as a potential therapeutic target to also overcome excessive T cell infiltration, which can exacerbate chronic liver disease progression.

CHAPTER 5: FUTURE DIRECTIONS

In this project, we were able to demonstrate $CD8^+$ and $CD4^+$ T cell hyperfunction in a diet-induced liver injury murine model, in addition to liver injury severity and infiltration. According to Matsumoto et al., in C57BL/6 mice, moderate inflammation and ballooning with advanced steatohepatitis (S3) are expected after 3 weeks of feeding, followed by moderate (F1-2) and advanced liver fibrosis (F3) by 6-9 and 12 weeks of feeding, respectively[126]. Due to a limited number of experimental mice, livers were only collected and stained for histology and triple IF at endpoint (20 weeks), and after returning to a regular chow diet for 4 weeks. It would be important to collect livers at the aforementioned timepoints throughout the experiment, in order to confirm the development of liver injury as expected. This would also allow us to associate liver injury with T cell hyperfunction and infiltration, with the addition of histological evidence to further support the flow cytometry results.

Another important experimental focus would be adding $CD4^+$ T cell subsets, specifically Th1, Th17 and Treg markers, to the flow cytometry and triple IF staining panels. Many studies have demonstrated that these subsets play important roles in the development of chronic liver disease. For example, in MASLD, a positive correlation was found between subsets of peripheral $CD4^+$ T cell subsets (Th1 and Th17) and the severity of liver injury (steatosis, hepatocyte ballooning and lobular inflammation)[70]. Furthermore, research done by Her et al, demonstrated that IL-17-secreting Th17 and IFN-γ-secreting Th1 cells play a key role in the progression of steatosis to fibrosis and correlate positively with disease progress in MASH-HCC[72]. The balance between Th17 and Tregs within the liver is also vital to disease progression, where Th17 produces pro-inflammatory cytokines via secretion of IL-17A, while Tregs relieves inflammation by suppressing T cell activation and differentiation[73,74]. By adding these subset markers to the staining

panels, it would allow us to study the relationship between these T cells and how its dysfunction, if evident, interplays with disease progression.

References

1. Asrani SK, Devarbhavi H, Eaton J, Kamath PS. Burden of liver diseases in the world. *Journal of Hepatology*. 2019;70(1):151-171. doi:10.1016/j.jhep.2018.09.014

2. How To Recognize Liver Disease. Cleveland Clinic. Accessed September 12, 2024. https://my.clevelandclinic.org/health/diseases/17179-liver-disease

3. Premkumar M, Anand AC. Overview of Complications in Cirrhosis. *J Clin Exp Hepatol*. 2022;12(4):1150-1174. doi:10.1016/j.jceh.2022.04.021

4. Global Cancer Statistics 2020: GLOBOCAN Estimates of Incidence and Mortality Worldwide for 36 Cancers in 185 Countries - Sung - 2021 - CA: A Cancer Journal for Clinicians - Wiley Online Library. Accessed May 24, 2024. https://acsjournals.onlinelibrary.wiley.com/doi/10.3322/caac.21660

5. Canada PHA of. Surveillance of hepatitis C. March 10, 2016. Accessed January 17, 2023. https://www.canada.ca/en/public-health/services/diseases/hepatitis-c/surveillance-hepatitis-c.html

6. Moon AM, Singal AG, Tapper EB. Contemporary Epidemiology of Chronic Liver Disease and Cirrhosis. *Clin Gastroenterol Hepatol*. 2020;18(12):2650-2666. doi:10.1016/j.cgh.2019.07.060

7. How Can Early Diagnosis of Fatty Liver be More Accurate and Accessible? Imaging Technology News. January 19, 2022. Accessed January 17, 2023. http://www.itnonline.com/content/how-can-early-diagnosis-fatty-liver-be-more-accurate-and-accessible

8. Vernon G, Baranova A, Younossi ZM. Systematic review: the epidemiology and natural history of non-alcoholic fatty liver disease and non-alcoholic steatohepatitis in adults. *Aliment Pharmacol Ther*. 2011;34(3):274-285. doi:10.1111/j.1365-2036.2011.04724.x

9. ND AM. Non-Alcoholic Fatty Liver Disease, an Overview. *Integr Med (Encinitas)*. 2019;18(2):42-49.

10. Axley P, Ahmed Z, Ravi S, Singal AK. Hepatitis C Virus and Hepatocellular Carcinoma: A Narrative Review. *Journal of Clinical and Translational Hepatology*. 2018;6(1):79-84. doi:10.14218/JCTH.2017.00067

11. Hoshida Y, Fuchs BC, Bardeesy N, Baumert TF, Chung RT. Pathogenesis and prevention of hepatitis C virus-induced hepatocellular carcinoma. *J Hepatol*. 2014;61(1 0):S79-S90. doi:10.1016/j.jhep.2014.07.010

12. Dhamija E, Paul SB, Kedia S. Non-alcoholic fatty liver disease associated with hepatocellular carcinoma: An increasing concern. *Indian J Med Res*. 2019;149(1):9-17. doi:10.4103/ijmr.IJMR_1456_17

13. Nasr P, Ignatova S, Kechagias S, Ekstedt M. Natural history of nonalcoholic fatty liver disease: A prospective follow-up study with serial biopsies. *Hepatol Commun*. 2018;2(2):199-210. doi:10.1002/hep4.1134

14. Zeisel MB, Barth H, Schuster C, Baumert TF. Hepatitis C virus entry: molecular mechanisms and targets for antiviral therapy. *Front Biosci (Landmark Ed)*. 2009;14:3274-3285.

15. Schaefer TJ, John S. Acute Hepatitis. In: *StatPearls*. StatPearls Publishing; 2024. Accessed July 24, 2024. http://www.ncbi.nlm.nih.gov/books/NBK551570/

16. Canada PHA of. Hepatitis C: For health professionals. March 10, 2016. Accessed September 12, 2024. https://www.canada.ca/en/public-health/services/diseases/hepatitis-c/health-professionals-hepatitis-c.html

17. Hepatitis C: Practice Essentials, Background, Pathophysiology. Published online June 5, 2024. Accessed July 24, 2024. https://emedicine.medscape.com/article/177792-overview?form=fpf#a3

18. Hofmann M, Tauber C, Hensel N, Thimme R. CD8+ T Cell Responses during HCV Infection and HCC. *J Clin Med*. 2021;10(5):991. doi:10.3390/jcm10050991

19. Schulze-Krebs A, Preimel D, Popov Y, et al. Hepatitis C virus-replicating hepatocytes induce fibrogenic activation of hepatic stellate cells. *Gastroenterology*. 2005;129(1):246-258. doi:10.1053/j.gastro.2005.03.089

20. Khatun M, Ray RB. Mechanisms Underlying Hepatitis C Virus-Associated Hepatic Fibrosis. *Cells*. 2019;8(10):1249. doi:10.3390/cells8101249

21. Luna-Cuadros MA, Chen HW, Hanif H, Ali MJ, Khan MM, Lau DTY. Risk of hepatocellular carcinoma after hepatitis C virus cure. *World J Gastroenterol*. 2022;28(1):96-107. doi:10.3748/wjg.v28.i1.96

22. Singal AG, Lim JK, Kanwal F. AGA Clinical Practice Update on Interaction between Oral Direct-Acting Antivirals (DAAs) for Chronic Hepatitis C Infection and Hepatocellular Carcinoma: Expert Review. *Gastroenterology*. 2019;156(8):2149-2157. doi:10.1053/j.gastro.2019.02.046

23. Knop V, Hoppe D, Welzel T, et al. Regression of fibrosis and portal hypertension in HCV-associated cirrhosis and sustained virologic response after interferon-free antiviral therapy. *J Viral Hepat*. 2016;23(12):994-1002. doi:10.1111/jvh.12578

24. Direct-acting antivirals for the treatment of hepatitis C virus infection - UpToDate. Accessed September 12, 2024. https://www.uptodate.com/contents/direct-acting-antivirals-for-the-treatment-of-hepatitis-c-virus-infection

25. Zeng H, Li L, Hou Z, Zhang Y, Tang Z, Liu S. Direct-acting Antiviral in the Treatment of Chronic Hepatitis C: Bonuses and Challenges. *Int J Med Sci*. 2020;17(7):892-902. doi:10.7150/ijms.43079

26. Li HC, Yang CH, Lo SY. Cellular factors involved in the hepatitis C virus life cycle. *World Journal of Gastroenterology*. 2021;27(28):4555-4581. doi:10.3748/wjg.v27.i28.4555

27. Luxenburger H, Neumann-Haefelin C, Thimme R, Boettler T. HCV-Specific T Cell Responses During and After Chronic HCV Infection. *Viruses*. 2018;10(11):645. doi:10.3390/v10110645

28. Capone F, Guerriero E, Colonna G, et al. Cytokinome profile evaluation in patients with hepatitis C virus infection. *World J Gastroenterol*. 2014;20(28):9261-9269. doi:10.3748/wjg.v20.i28.9261

29. Shrivastava S, Mukherjee A, Ray R, Ray RB. Hepatitis C virus induces interleukin-1β (IL-1β)/IL-18 in circulatory and resident liver macrophages. *J Virol*. 2013;87(22):12284-12290. doi:10.1128/JVI.01962-13

30. Sung PS, Racanelli V, Shin EC. CD8+ T-Cell Responses in Acute Hepatitis C Virus Infection. *Front Immunol*. 2014;5:266. doi:10.3389/fimmu.2014.00266

31. Quarleri JF, Oubiña JR. Hepatitis C virus strategies to evade the specific-T cell response: a possible mission favoring its persistence. *Ann Hepatol*. 2016;15(1):17-26. doi:10.5604/16652681.1184193

32. Aslan N, Yurdaydin C, Wiegand J, et al. Cytotoxic CD4+ T cells in viral hepatitis. *Journal of Viral Hepatitis*. 2006;13(8):505-514. doi:10.1111/j.1365-2893.2006.00723.x

33. Maehara T, Kaneko N, Perugino CA, et al. Cytotoxic CD4+ T lymphocytes may induce endothelial cell apoptosis in systemic sclerosis. *J Clin Invest*. 130(5):2451-2464. doi:10.1172/JCI131700

34. Schulze Zur Wiesch J, Ciuffreda D, Lewis-Ximenez L, et al. Broadly directed virus-specific CD4+ T cell responses are primed during acute hepatitis C infection, but rapidly disappear from human blood with viral persistence. *J Exp Med*. 2012;209(1):61-75. doi:10.1084/jem.20100388

35. Malyshkina A, Brüggemann A, Paschen A, Dittmer U. Cytotoxic CD4+ T cells in chronic viral infections and cancer. *Front Immunol*. 2023;14. doi:10.3389/fimmu.2023.1271236

36. Barber DL, Wherry EJ, Masopust D, et al. Restoring function in exhausted CD8 T cells during chronic viral infection. *Nature*. 2006;439(7077):682-687. doi:10.1038/nature04444

37. Women living with hepatitis - World Hepatitis Alliance. March 6, 2024. Accessed September 13, 2024. https://www.worldhepatitisalliance.org/women/, https://www.worldhepatitisalliance.org/women/

38. Abdel-Gawad M, Nour M, El-Raey F, Nagdy H, Almansoury Y, El-Kassas M. Gender differences in prevalence of hepatitis C virus infection in Egypt: a systematic review and meta-analysis. *Sci Rep*. 2023;13(1):2499. doi:10.1038/s41598-023-29262-z

39. Different effects of menopausal hormone therapy on non-alcoholic fatty liver disease based on the route of estrogen administration | Scientific Reports. Accessed July 29, 2024. https://www.nature.com/articles/s41598-023-42788-6

40. Baden R, Rockstroh JK, Buti M. Natural History and Management of Hepatitis C: Does Sex Play a Role? *The Journal of Infectious Diseases*. 2014;209(suppl_3):S81-S85. doi:10.1093/infdis/jiu057

41. Yuan Y, Shimizu I, Shen M, et al. Effects of estradiol and progesterone on the proinflammatory cytokine production by mononuclear cells from patients with chronic hepatitis C. *World J Gastroenterol*. 2008;14(14):2200-2207. doi:10.3748/wjg.14.2200

42. Progression of liver fibrosis in women infected with hepatitis C: long-term benefit of estrogen exposure - PubMed. Accessed July 29, 2024. https://pubmed.ncbi.nlm.nih.gov/15565616/

43. Florian R, Aye L, Mai S. Gender Differences in Outcomes of Patients Receiving Hepatitis C Treatment: A Single Center Experience: 2767. *Official journal of the American College of Gastroenterology | ACG*. 2017;112:S1496.

44. Younossi ZM, Koenig AB, Abdelatif D, Fazel Y, Henry L, Wymer M. Global epidemiology of nonalcoholic fatty liver disease—Meta-analytic assessment of prevalence, incidence, and outcomes. *Hepatology*. 2016;64(1):73. doi:10.1002/hep.28431

45. Teng ML, Ng CH, Huang DQ, et al. Global incidence and prevalence of nonalcoholic fatty liver disease. *Clin Mol Hepatol*. 2023;29(Suppl):S32-S42. doi:10.3350/cmh.2022.0365

46. Phoolchund AGS, Khakoo SI. MASLD and the Development of HCC: Pathogenesis and Therapeutic Challenges. *Cancers*. 2024;16(2):259. doi:10.3390/cancers16020259

47. A multisociety Delphi consensus statement on new fatty liver disease nomenclature - Journal of Hepatology. Accessed July 22, 2024. https://www.journal-of-hepatology.eu/article/S0168-8278(23)00418-X/fulltext

48. AASLD Practice Guidance on the clinical assessment and management of nonalcoholic fatty liver disease - PubMed. Accessed July 22, 2024. https://pubmed.ncbi.nlm.nih.gov/36727674/

49. Kohli R, Kirby M, Xanthakos SA, et al. High-fructose, medium chain trans fat diet induces liver fibrosis and elevates plasma coenzyme Q9 in a novel murine model of obesity and nonalcoholic steatohepatitis. *Hepatology*. 2010;52(3):934-944. doi:10.1002/hep.23797

50. Long-Term Adverse Effect of Liver Stiffness on Glycaemic Control in Type 2 Diabetic Patients with Nonalcoholic Fatty Liver Disease: A Pilot Study - PubMed. Accessed July 23, 2024. https://pubmed.ncbi.nlm.nih.gov/36293337/

51. Pierantonelli I, Svegliati-Baroni G. Nonalcoholic Fatty Liver Disease: Basic Pathogenetic Mechanisms in the Progression From NAFLD to NASH. *Transplantation*. 2019;103(1):e1-e13. doi:10.1097/TP.0000000000002480

52. Byrne CD, Targher G. NAFLD: a multisystem disease. *J Hepatol*. 2015;62(1 Suppl):S47-64. doi:10.1016/j.jhep.2014.12.012

53. Metabolic Dysfunction–Associated Liver Disease (MASLD) - Hepatic and Biliary Disorders. Merck Manual Professional Edition. Accessed July 23, 2024. https://www.merckmanuals.com/en-ca/professional/hepatic-and-biliary-disorders/approach-to-the-patient-with-liver-disease/metabolic-dysfunction–associated-liver-disease-masld

54. Cassinotto C, Boursier J, de Lédinghen V, et al. Liver stiffness in nonalcoholic fatty liver disease: A comparison of supersonic shear imaging, FibroScan, and ARFI with liver biopsy. *Hepatology*. 2016;63(6):1817-1827. doi:10.1002/hep.28394

55. Lee MS, Bae JM, Joo SK, et al. Prospective comparison among transient elastography, supersonic shear imaging, and ARFI imaging for predicting fibrosis in nonalcoholic fatty liver disease. *PLoS One*. 2017;12(11):e0188321. doi:10.1371/journal.pone.0188321

56. Fibrosis of the Liver - Liver and Gallbladder Disorders. Merck Manuals Consumer Version. Accessed January 17, 2023. https://www.merckmanuals.com/en-ca/home/liver-and-gallbladder-disorders/fibrosis-and-cirrhosis-of-the-liver/fibrosis-of-the-liver

57. Koutoukidis DA, Koshiaris C, Henry JA, et al. The effect of the magnitude of weight loss on non-alcoholic fatty liver disease: A systematic review and meta-analysis. *Metabolism*. 2021;115:154455. doi:10.1016/j.metabol.2020.154455

58. Hashida R, Kawaguchi T, Bekki M, et al. Aerobic vs. resistance exercise in non-alcoholic fatty liver disease: A systematic review. *J Hepatol*. 2017;66(1):142-152. doi:10.1016/j.jhep.2016.08.023

59. Zhou XD, Wong VWS, Zheng MH. Resmetirom and GLP-1 agonists for MASH: complementary rather than exclusive. *npj Gut Liver*. 2024;1(1):1-3. doi:10.1038/s44355-024-00004-w

60. Harrison SA, Bedossa P, Guy CD, et al. A Phase 3, Randomized, Controlled Trial of Resmetirom in NASH with Liver Fibrosis. *N Engl J Med*. 2024;390(6):497-509. doi:10.1056/NEJMoa2309000

61. Harrison SA, Taub R, Neff GW, et al. Resmetirom for nonalcoholic fatty liver disease: a randomized, double-blind, placebo-controlled phase 3 trial. *Nat Med*. 2023;29(11):2919-2928. doi:10.1038/s41591-023-02603-1

62. Canadian Liver Foundation: Fatty liver disease treatment approved in U.S. signals new era for Canadians. Healthing.ca. Accessed September 18, 2024. https://www.healthing.ca/wellness/opinion/canadian-liver-foundation-fatty-liver-disease-treatment-approved-in-u-s-signals-new-era-for-canadians

63. Abushamat LA, Shah PA, Eckel RH, Harrison SA, Barb D. The Emerging Role of Glucagon-Like Peptide-1 Receptor Agonists for the Treatment of Metabolic Dysfunction-Associated Steatohepatitis. *Clinical Gastroenterology and Hepatology*. 2024;22(8):1565-1574. doi:10.1016/j.cgh.2024.01.032

64. Noureddin M. MASH clinical trials and drugs pipeline: An impending tsunami. *Hepatology*. Published online March 19, 2024. doi:10.1097/HEP.0000000000000860

65. Role of nonresolving inflammation in hepatocellular carcinoma development and progression | npj Precision Oncology. Accessed July 23, 2024. https://www.nature.com/articles/s41698-018-0048-z

66. Koyama Y, Brenner DA. Liver inflammation and fibrosis. *J Clin Invest*. 2017;127(1):55-64. doi:10.1172/JCI88881

67. The Differential Roles of T Cells in Non-alcoholic Fatty Liver Disease and Obesity - PubMed. Accessed July 22, 2024. https://pubmed.ncbi.nlm.nih.gov/30787925/

68. McVey JC, Green BL, Ruf B, et al. NAFLD indirectly impairs antigen-specific CD8+ T cell immunity against liver cancer in mice. *iScience*. 2022;25(2):103847. doi:10.1016/j.isci.2022.103847

69. Zhang M, Zhang S. T Cells in Fibrosis and Fibrotic Diseases. *Front Immunol*. 2020;11. doi:10.3389/fimmu.2020.01142

70. Haas JT, Vonghia L, Mogilenko DA, et al. Transcriptional network analysis implicates altered hepatic immune function in NASH development and resolution. *Nat Metab*. 2019;1(6):604-614. doi:10.1038/s42255-019-0076-1

71. Levinsson A, Zolopa C, Vakili F, et al. Sex and gender differences in hepatitis C virus risk, prevention, and cascade of care in people who inject drugs: systematic review and meta-analysis. *eClinicalMedicine*. 2024;72. doi:10.1016/j.eclinm.2024.102596

72. Her Z, Tan JHL, Lim YS, et al. CD4+ T Cells Mediate the Development of Liver Fibrosis in High Fat Diet-Induced NAFLD in Humanized Mice. *Frontiers in Immunology*. 2020;11. Accessed January 17, 2023. https://www.frontiersin.org/articles/10.3389/fimmu.2020.580968

73. Wang H, Tsung A, Mishra L, Huang H. Regulatory T cell: a double-edged sword from metabolic-dysfunction-associated steatohepatitis to hepatocellular carcinoma. *eBioMedicine*. 2024;101:105031. doi:10.1016/j.ebiom.2024.105031

74. Li K, Liu H, Guo T. Th17/Treg imbalance is an indicator of liver cirrhosis process and a risk factor for HCC occurrence in HBV patients. *Clinics and Research in Hepatology and Gastroenterology*. 2017;41(4):399-407. doi:10.1016/j.clinre.2016.12.004

75. Woestemeier A, Scognamiglio P, Zhao Y, et al. Multicytokine-producing $CD4^+$ T cells characterize the livers of patients with NASH. *JCI Insight*. 2023;8(1). doi:10.1172/jci.insight.153831

76. Mao T, Yang R, Luo Y, He K. Crucial role of T cells in NAFLD-related disease: A review and prospect. *Front Endocrinol (Lausanne)*. 2022;13:1051076. doi:10.3389/fendo.2022.1051076

77. Hirsova P, Bamidele AO, Wang H, Povero D, Revelo XS. Emerging Roles of T Cells in the Pathogenesis of Nonalcoholic Steatohepatitis and Hepatocellular Carcinoma. *Front Endocrinol (Lausanne)*. 2021;12:760860. doi:10.3389/fendo.2021.760860

78. Younossi ZM, Golabi P, Paik JM, Henry A, Van Dongen C, Henry L. The global epidemiology of nonalcoholic fatty liver disease (NAFLD) and nonalcoholic steatohepatitis (NASH): a systematic review. *Hepatology*. 2023;77(4):1335-1347. doi:10.1097/HEP.0000000000000004

79. Ji H, Cheng S, Yeo YH, Trivedi H, Reue K, Kwan A. Sex differences in prevalence and prognosis of steatotic liver disease phenotypes: Biological sex matters. *Journal of Hepatology*. 2024;80(2):e68-e69. doi:10.1016/j.jhep.2023.08.013

80. Cherubini A, Della Torre S, Pelusi S, Valenti L. Sexual dimorphism of metabolic dysfunction-associated steatotic liver disease. *Trends in Molecular Medicine*. Published online June 17, 2024. doi:10.1016/j.molmed.2024.05.013

81. Ballestri S, Nascimbeni F, Baldelli E, Marrazzo A, Romagnoli D, Lonardo A. NAFLD as a Sexual Dimorphic Disease: Role of Gender and Reproductive Status in the Development and Progression of Nonalcoholic Fatty Liver Disease and Inherent Cardiovascular Risk. *Adv Ther*. 2017;34(6):1291-1326. doi:10.1007/s12325-017-0556-1

82. Burra P, Bizzaro D, Gonta A, et al. Clinical impact of sexual dimorphism in non-alcoholic fatty liver disease (NAFLD) and non-alcoholic steatohepatitis (NASH). *Liver International*. 2021;41(8):1713-1733. doi:10.1111/liv.14943

83. Florio AA, Graubard BI, Yang B, et al. Oophorectomy and risk of non-alcoholic fatty liver disease and primary liver cancer in the Clinical Practice Research Datalink. *Eur J Epidemiol*. 2019;34(9):871-878. doi:10.1007/s10654-019-00526-1

84. Aldhoon-Hainerová I, Zamrazilová H, Hill M, Hainer V. Insulin sensitivity and its relation to hormones in adolescent boys and girls. *Metabolism*. 2017;67:90-98. doi:10.1016/j.metabol.2016.10.005

85. Sex Differences in Nonalcoholic Fatty Liver Disease: Estrogen Influence on the Liver–Adipose Tissue Crosstalk | Antioxidants & Redox Signaling. Accessed July 24, 2024. https://www.liebertpub.com/doi/10.1089/ars.2021.0044

86. Zidon TM, Padilla J, Fritsche KL, et al. Effects of ERβ and ERα on OVX-induced changes in adiposity and insulin resistance. Published online April 1, 2020. doi:10.1530/JOE-19-0321

87. Cells | Free Full-Text | Beyond the X Factor: Relevance of Sex Hormones in NAFLD Pathophysiology. Accessed July 24, 2024. https://www.mdpi.com/2073-4409/10/9/2502

88. Yang JD, Abdelmalek MF, Guy CD, et al. Patient Sex, Reproductive Status, and Synthetic Hormone Use Associate With Histologic Severity of Nonalcoholic Steatohepatitis. *Clinical Gastroenterology and Hepatology*. 2017;15(1):127-131.e2. doi:10.1016/j.cgh.2016.07.034

89. Wong EA, Joslyn L, Grant NL, et al. Low Levels of T Cell Exhaustion in Tuberculous Lung Granulomas. *Infect Immun*. 2018;86(9):e00426-18. doi:10.1128/IAI.00426-18

90. Gigley JP, Bhadra R, Moretto MM, Khan IA. T Cell exhaustion in protozoan disease. *Trends Parasitol*. 2012;28(9):377-384. doi:10.1016/j.pt.2012.07.001

91. T-cell exhaustion: characteristics, causes and conversion - PubMed. Accessed July 30, 2024. https://pubmed.ncbi.nlm.nih.gov/20201977/

92. Wherry EJ, Blattman JN, Murali-Krishna K, van der Most R, Ahmed R. Viral persistence alters CD8 T-cell immunodominance and tissue distribution and results in distinct stages of functional impairment. *J Virol*. 2003;77(8):4911-4927. doi:10.1128/jvi.77.8.4911-4927.2003

93. Topchyan P, Lin S, Cui W. The Role of CD4 T Cell Help in CD8 T Cell Differentiation and Function During Chronic Infection and Cancer. *Immune Network*. 2023;23(5). doi:10.4110/in.2023.23.e41

94. Fröhlich A, Kisielow J, Schmitz I, et al. IL-21R on T cells is critical for sustained functionality and control of chronic viral infection. *Science*. 2009;324(5934):1576-1580. doi:10.1126/science.1172815

95. Spaan M, Kreefft K, de Graav GN, et al. CD4+ CXCR5+ T cells in chronic HCV infection produce less IL-21, yet are efficient at supporting B cell responses. *J Hepatol*. 2015;62(2):303-310. doi:10.1016/j.jhep.2014.09.024

96. Kurachi M. CD8+ T cell exhaustion. *Semin Immunopathol*. 2019;41(3):327-337. doi:10.1007/s00281-019-00744-5

97. McLane LM, Abdel-Hakeem MS, Wherry EJ. CD8 T Cell Exhaustion During Chronic Viral Infection and Cancer. *Annu Rev Immunol*. 2019;37:457-495. doi:10.1146/annurev-immunol-041015-055318

98. Abdel-Hakeem MS, Manne S, Beltra JC, et al. Epigenetic scarring of exhausted T cells hinders memory differentiation upon eliminating chronic antigenic stimulation. *Nat Immunol*. 2021;22(8):1008-1019. doi:10.1038/s41590-021-00975-5

99. Vranjkovic A, Deonarine F, Kaka S, Angel JB, Cooper CL, Crawley AM. Direct-Acting Antiviral Treatment of HCV Infection Does Not Resolve the Dysfunction of Circulating CD8+ T-Cells in Advanced Liver Disease. *Front Immunol*. 2019;10:1926. doi:10.3389/fimmu.2019.01926

100. Madani J, Li J, Vranjkovic A, et al. CD8 T cell hyperfunction and reduced tumour control in models of advanced liver fibrosis. Published online September 22, 2023:2023.09.20.557752. doi:10.1101/2023.09.20.557752

101. Li J, Vranjkovic A, Read D, et al. Lasting differential gene expression of circulating CD8 T cells in chronic HCV infection with cirrhosis identifies a role for Hedgehog signaling in cellular hyperfunction. *Front Immunol*. 2024;15:1375485. doi:10.3389/fimmu.2024.1375485

102. NAFLD causes selective CD4+ T lymphocyte loss and promotes hepatocarcinogenesis | Nature. Accessed July 23, 2024. https://www.nature.com/articles/nature16969

103. Jorritsma K. *CD8+ T Cell Hyperfunction and Immunometabolism in Murine Models of Chronic Liver Disease*. Université d'Ottawa | University of Ottawa; 2024. Accessed September 18, 2024. http://hdl.handle.net/10393/46091

104. Lee S, Kwak JH, Kim SH, et al. Comparative study of liver injury induced by high-fat methionine- and choline-deficient diet in ICR mice originating from three different sources. *Laboratory Animal Research*. 2019;35(1):15. doi:10.1186/s42826-019-0016-y

105. Karlmark KR, Wasmuth HE, Trautwein C, Tacke F. Chemokine-directed immune cell infiltration in acute and chronic liver disease. *Expert Rev Gastroenterol Hepatol*. 2008;2(2):233-242. doi:10.1586/17474124.2.2.233

106. Claassen MAA, de Knegt RJ, Tilanus HW, Janssen HLA, Boonstra A. Abundant numbers of regulatory T cells localize to the liver of chronic hepatitis C infected patients and limit the extent of fibrosis. *Journal of Hepatology*. 2010;52(3):315-321. doi:10.1016/j.jhep.2009.12.013

107. Ward SM, Fox BC, Brown PJ, et al. Quantification and localisation of FOXP3+ T lymphocytes and relation to hepatic inflammation during chronic HCV infection. *J Hepatol*. 2007;47(3):316-324. doi:10.1016/j.jhep.2007.03.023

108. Radziewicz H, Ibegbu CC, Fernandez ML, et al. Liver-Infiltrating Lymphocytes in Chronic Human Hepatitis C Virus Infection Display an Exhausted Phenotype with High Levels of PD-1 and Low Levels of CD127 Expression. *Journal of Virology*. 2007;81(6):2545-2553. doi:10.1128/jvi.02021-06

109. Russell JQ, Morrissette GJ, Weidner M, Vyas C, Aleman-Hoey D, Budd RC. Liver Damage Preferentially Results from CD8+ T Cells Triggered by High Affinity Peptide Antigens. *J Exp Med*. 1998;188(6):1147-1157.

110. Wang Y, Zhang C. The Roles of Liver-Resident Lymphocytes in Liver Diseases. *Front Immunol*. 2019;10:1582. doi:10.3389/fimmu.2019.01582

111. Schuster S, Cabrera D, Arrese M, Feldstein AE. Triggering and resolution of inflammation in NASH. *Nat Rev Gastroenterol Hepatol*. 2018;15(6):349-364. doi:10.1038/s41575-018-0009-6

112. Bai J, Zhu L, Mi W, et al. Multiscale integrative analyses unveil immune-related diagnostic signature for the progression of MASLD. *Hepatol Commun*. 2023;7(11):e0298. doi:10.1097/HC9.0000000000000298

113. Sutti S, Jindal A, Locatelli I, et al. Adaptive immune responses triggered by oxidative stress contribute to hepatic inflammation in NASH. *Hepatology*. 2014;59(3):886-897. doi:10.1002/hep.26749

114. Wolf MJ, Adili A, Piotrowitz K, et al. Metabolic activation of intrahepatic CD8+ T cells and NKT cells causes nonalcoholic steatohepatitis and liver cancer via cross-talk with hepatocytes. *Cancer Cell*. 2014;26(4):549-564. doi:10.1016/j.ccell.2014.09.003

115. Grohmann M, Wiede F, Dodd GT, et al. Obesity Drives STAT-1-Dependent NASH and STAT-3-Dependent HCC. *Cell*. 2018;175(5):1289-1306.e20. doi:10.1016/j.cell.2018.09.053

116. Seike T, Mizukoshi E, Kaneko S. Role of CD4+ T-cells in the pathology of non-alcoholic fatty liver disease and related diseases. *hr*. 2021;7(0):N/A-N/A. doi:10.20517/2394-5079.2021.46

117. Gomes AL, Teijeiro A, Burén S, et al. Metabolic Inflammation-Associated IL-17A Causes Non-alcoholic Steatohepatitis and Hepatocellular Carcinoma. *Cancer Cell*. 2016;30(1):161-175. doi:10.1016/j.ccell.2016.05.020

118. Scholten D, Trebicka J, Liedtke C, Weiskirchen R. The carbon tetrachloride model in mice. *Lab Anim*. 2015;49(1_suppl):4-11. doi:10.1177/0023677215571192

119. Fujii T, Fuchs BC, Yamada S, et al. Mouse model of carbon tetrachloride induced liver fibrosis: Histopathological changes and expression of CD133 and epidermal growth factor. *BMC Gastroenterology*. 2010;10(1):79. doi:10.1186/1471-230X-10-79

120. Wolf CR, Harrelson WG, Nastainczyk WM, Philpot RM, Kalyanaraman B, Mason RP. Metabolism of carbon tetrachloride in hepatic microsomes and reconstituted monooxygenase systems and its relationship to lipid peroxidation. *Mol Pharmacol*. 1980;18(3):553-558.

121. Weiskirchen R, Weiskirchen S, Tacke F. Recent advances in understanding liver fibrosis: bridging basic science and individualized treatment concepts. Published online June 27, 2018. doi:10.12688/f1000research.14841.1

122. Starkel P, Leclercq IA. Animal models for the study of hepatic fibrosis. *Best Pract Res Clin Gastroenterol*. 2011;25(2):319-333. doi:10.1016/j.bpg.2011.02.004

123. Anstee QM, Goldin RD. Mouse models in non-alcoholic fatty liver disease and steatohepatitis research. *Int J Exp Pathol*. 2006;87(1):1-16. doi:10.1111/j.0959-9673.2006.00465.x

124. Kleiner DE, Brunt EM, Van Natta M, et al. Design and validation of a histological scoring system for nonalcoholic fatty liver disease. *Hepatology*. 2005;41(6):1313-1321. doi:10.1002/hep.20701

125. Denda A, Kitayama W, Kishida H, et al. Development of hepatocellular adenomas and carcinomas associated with fibrosis in C57BL/6J male mice given a choline-deficient, L-amino acid-defined diet. *Jpn J Cancer Res*. 2002;93(2):125-132. doi:10.1111/j.1349-7006.2002.tb01250.x

126. Matsumoto M, Hada N, Sakamaki Y, et al. An improved mouse model that rapidly develops fibrosis in non-alcoholic steatohepatitis. *Int J Exp Pathol*. 2013;94(2):93-103. doi:10.1111/iep.12008

127. A06071302 Formula - Search Formulas - Research Diets, Inc. Accessed June 13, 2024. https://researchdiets.com/formulas/a06071302

128. 2018 Teklad Global 18% Protein Rodent Diets. Accessed June 13, 2024. https://www.inotivco.com/rodent-natural-ingredient-2018-diets

129. Yang CR, Lin WJ, Shen PC, et al. Phenotypic and metabolomic characteristics of mouse models of metabolic associated steatohepatitis. *Biomark Res*. 2024;12:6. doi:10.1186/s40364-023-00555-9

130. Weijers G, Munsterman ID, Thijssen JM, Kuppeveld H, Drenth JPH. Noninvasive Staging of Hepatic Steatosis Using Calibrated 2D US with Liver Biopsy as the Reference Standard. 2023;306(3).

131. EasySep™ Human CD4 Positive Selection Kit II | STEMCELL Technologies. Accessed June 14, 2024. https://www.stemcell.com/products/easysep-human-cd4-positive-selection-kit-ii.html

132. Li Z, Wang S, Xu Q, et al. The double roles of T cell-mediated immune response in the progression of MASLD. *Biomedicine & Pharmacotherapy*. 2024;173:116333. doi:10.1016/j.biopha.2024.116333

133. Liver fibrosis quantification - PMC. Accessed June 19, 2024. https://www.ncbi.nlm.nih.gov/pmc/articles/PMC9538706/

134. Xin X, Cai BY, Chen C, et al. High-trans fatty acid and high-sugar diets can cause mice with non-alcoholic steatohepatitis with liver fibrosis and potential pathogenesis. *Nutrition & Metabolism*. 2020;17(1):40. doi:10.1186/s12986-020-00462-y

135. Zhong F, Zhou X, Xu J, Gao L. Rodent Models of Nonalcoholic Fatty Liver Disease. *Digestion*. 2020;101(5):522-535. doi:10.1159/000501851

136. Lonardo A, Nascimbeni F, Ballestri S, et al. Sex Differences in NAFLD: State of the Art and Identification of Research Gaps. *Hepatology*. 2019;70(4):1457-1469. doi:10.1002/hep.30626

137. Ong JP, Pitts A, Younossi ZM. Increased overall mortality and liver-related mortality in non-alcoholic fatty liver disease. *J Hepatol*. 2008;49(4):608-612. doi:10.1016/j.jhep.2008.06.018

138. Cao L, An Y, Liu H, et al. Global epidemiology of type 2 diabetes in patients with NAFLD or MAFLD: a systematic review and meta-analysis. *BMC Medicine*. 2024;22(1):101. doi:10.1186/s12916-024-03315-0

139. Møhlenberg M, Terczynska-Dyla E, Thomsen KL, et al. The role of IFN in the development of NAFLD and NASH. *Cytokine*. 2019;124:154519. doi:10.1016/j.cyto.2018.08.013

140. Chen Q, Yi J, Liu F, et al. TGF-β1 contributes to the hepatic inflammation in animal models with nonalcoholic steatohepatitis by Smad3/TLR2 signaling pathway. *Molecular Immunology*. 2022;152:129-139. doi:10.1016/j.molimm.2022.10.014

141. Kim SE, Min JS, Lee S, Lee DY, Choi D. Different effects of menopausal hormone therapy on non-alcoholic fatty liver disease based on the route of estrogen administration. *Sci Rep*. 2023;13:15461. doi:10.1038/s41598-023-42788-6

142. Dong S, Chen QL, Song YN, et al. Mechanisms of CCl4-induced liver fibrosis with combined transcriptomic and proteomic analysis. *J Toxicol Sci*. 2016;41(4):561-572. doi:10.2131/jts.41.561

143. Keenan BP, Fong L, Kelley RK. Immunotherapy in hepatocellular carcinoma: the complex interface between inflammation, fibrosis, and the immune response. *J Immunother Cancer*. 2019;7(1):267. doi:10.1186/s40425-019-0749-z

144. Xu JW, Gong J, Chang XM, et al. Estrogen reduces CCL4- induced liver fibrosis in rats. *World J Gastroenterol*. 2002;8(5):883-887. doi:10.3748/wjg.v8.i5.883

145. Collazos J, Pérez-Is L, de la Fuente B, et al. No gender differences in the 24-month course of non-invasive liver fibrosis markers after DAA therapy in HCV-mono and HCV/HIV-coinfected patients. *Sci Rep*. 2024;14(1):7534. doi:10.1038/s41598-024-57845-x

146. Osuch S, Laskus T, Berak H, et al. Decrease of T-cells exhaustion markers programmed cell death-1 and T-cell immunoglobulin and mucin domain-containing protein 3 and plasma

IL-10 levels after successful treatment of chronic hepatitis C. *Sci Rep*. 2020;10(1):16060. doi:10.1038/s41598-020-73137-6

147. Boldogh I, Albrecht T, Porter DD. Persistent Viral Infections. In: Baron S, ed. *Medical Microbiology*. 4th ed. University of Texas Medical Branch at Galveston; 1996. Accessed July 30, 2024. http://www.ncbi.nlm.nih.gov/books/NBK8538/

148. Matloubian M, Concepcion RJ, Ahmed R. CD4+ T cells are required to sustain CD8+ cytotoxic T-cell responses during chronic viral infection. *J Virol*. 1994;68(12):8056-8063. doi:10.1128/JVI.68.12.8056-8063.1994

149. CD8+ T-Cell Responses in Acute Hepatitis C Virus Infection - PMC. Accessed August 27, 2024. https://www.ncbi.nlm.nih.gov/pmc/articles/PMC4047488/

150. Sun XF, Gu L, Deng WS, Xu Q. Impaired balance of T helper 17/T regulatory cells in carbon tetrachloride-induced liver fibrosis in mice. *World J Gastroenterol*. 2014;20(8):2062-2070. doi:10.3748/wjg.v20.i8.2062

151. Diaz Brinton R. Minireview: Translational Animal Models of Human Menopause: Challenges and Emerging Opportunities. *Endocrinology*. 2012;153(8):3571-3578. doi:10.1210/en.2012-1340

152. What Is Metabolic Dysfunction-Associated Steatotic Liver Disease? Cleveland Clinic. Accessed September 3, 2024. https://my.clevelandclinic.org/health/diseases/22437-non-alcoholic-fatty-liver-disease

153. Horng HC, Chang WH, Yeh CC, et al. Estrogen Effects on Wound Healing. *Int J Mol Sci*. 2017;18(11):2325. doi:10.3390/ijms18112325

154. NASH Definition & Progression. June 10, 2022. Accessed August 28, 2024. https://liverfoundation.org/liver-diseases/fatty-liver-disease/nonalcoholic-steatohepatitis-nash/nash-definition-prevalence/

155. Whittington NC, Wray S. Suppression of Red Blood Cell Autofluorescence for Immunocytochemistry on Fixed Embryonic Mouse Tissue. *Curr Protoc Neurosci*. 2017;81:2.28.1-2.28.12. doi:10.1002/cpns.35

156. Cuño-Gómiz C, de Gregorio E, Tutusaus A, et al. Sex-based differences in natural killer T cell-mediated protection against diet-induced steatohepatitis in Balb/c mice. *Biology of Sex Differences*. 2023;14(1):85. doi:10.1186/s13293-023-00569-w

157. Cueto-Sanchez A, Niu H, Del Campo-Herrera E, et al. Lymphocyte Profile and Immune Checkpoint Expression in Drug-Induced Liver Injury: An Immunophenotyping Study. *Clin Pharmacol Ther*. 2021;110(6):1604-1612. doi:10.1002/cpt.2423